UNIVERSITY OF COPENHAGEN
FACULTY OF SCIENCE

MSc in Physics

Experimental study of bacterial cell shape's role in competition: elongated cells win in expanding mixed communities

Nathánaël van den Berg

Supervised by Liselotte Jauffred and Namiko Mitarai

May 31, 2023

Nathánaël van den Berg

Experimental study of bacterial cell shape's role in competition: elongated cells win in expanding mixed communities

MSc in Physics, May 31, 2023

Supervisors: Liselotte Jauffred and Namiko Mitarai

University of Copenhagen

Faculty of Science

Masters Degree Physics

Blegdamsvej 17

2100 Copenhagen N

Acknowledgements

First and foremost I would like to express my thanks to Liselotte Jauffred and Namiko Mitarai for their invaluable guidance and support on this fun and challenging project. Special thanks to Alba García Vázquez for her daily advice and training, which have been crucial in shaping my skills in the lab. I am grateful to Trang Nguyen for her collaboration and joint efforts in conducting experiments. I thank Gerard van Schie for his coding tips. I would also like to acknowledge the Applied Statistics course for some of the fitting scripts I used. I extend my thanks to all the other people in our office, the A-floor, and the wider biocomplexity department for their support and the enjoyable atmosphere we've had while working together. Lastly, I would like to thank my friends and family for their support and interest in this project.

Abstract

Biofilms are diverse microbial communities that express complex mechanisms and structures such as the extracellular matrix. They are notorious for their impact on many human activities. Competing bacterial strains with different aspect ratios are known to form complex patterns and sort vertically within such communities. However, little is known about the cell shape's effect on competition and horizontal biofilm expansion. In this thesis, I study how bacterial shapes can lead to a competitive advantage in biofilm growth. I measured the growth rates of long and short *E. coli* mutants in a liquid medium and found them to be equal. Contrarily, I found that the expansion rate on a surface was more than twice as high for the elongated cells. I performed experiments where I mixed the two strains under various conditions to investigate how their competition leads to pattern formation. I found and quantified that long cells always dominate on a macroscopic scale, even when inoculated at much lower concentrations than short ones. My timelapse-microscopy work could be used as a starting point for studying evolutionary diversity or give insights into combating or utilizing biofilms.

Contents

1 Introduction

1.1 Motivation

To explain how we arrived at the starting point of my thesis, I must first talk about the biological background.

Bacteria are prokaryotic organisms, i.e. single-celled organisms without a nucleus and other membrane-bound organelles. Their genetic information is contained in a single loop of DNA. Some bacteria have additional loops of DNA called plasmids that allow them to express additional traits.

There exist many different kinds of bacteria with many different phenotypes. Their sizes can range from 0.5 to 5 micrometer and their shapes can vary from the common round cocci and cylindrical bacilli to much more exotic shapes. They exist in all habitats on Earth. This includes extremely cold, hot, acidic, and basic environments as well as the insides and outsides of plants and animals.

Bacteria are useful in many ways. Examples of applications are sewage treatment, fermentation, farming, and the production of medicine and biomolecules. They also live in the human body, primarily in the gut, and play an important role in our health. On the other hand, they can also be harmful parasites or pathogens and fast growth can cause problems rapidly. [1]

1.1.1 *Escherichia coli*

E. coli is the bacterial species used in this project. It is a commonly used species because it serves as a model system in microbiology [2]. *E. coli* is Gram-negative, meaning that it has an outer membrane besides its peptidoglycan layer and plasma membrane. It is anaerobic. This independence from oxygen allows it to

live in one of its favorite habitats: the human gut. The cells are rod-shaped with typical diameters of 0.8–$1\,\mu\mathrm{m}$ and lengths of 2–$4\,\mu\mathrm{m}$.

Populations can grow fast due to the short generation time of about twenty minutes (in good growth conditions). This allows for many generations to be studied in a short time. The species has low nutritional requirements and grows optimally at $37\,^{\circ}\mathrm{C}$. In this thesis, I use variants of the REL606 strain, a variant of the B laboratory strain used by Delbruck and Luria in 1940 [3]. This strain has limited motility due to its lack of flagella.

1.1.2 Biofilms

Under certain conditions, such as on surfaces with sufficient nutrients, bacteria can organize into communities commonly referred to as biofilms. These biofilms are typically dense colonies where the cells are physically touching. Many kinds of collaborations happen within most biofilms. Even different species can coexist within one colony, often with specific tasks.

One example of cooperation is the production of a so-called extracellular matrix. This is a network of fibrous proteins and other molecules that provides the collective with a mechanical structure and protection against environmental stresses, predation, and antibiotics. Other examples are the sharing of nutrients and communication between individual cells and regions of a colony. Competition within biofilms has also been observed and can promote evolutionary diversity. Flemming et al. [4] give a more thorough review of the known emergent properties of biofilms' communal lifestyle.

The growth in bacterial communities is typically different from that in liquid media. This is partially due to the interactions between cells and partially due to spatial constraints. With solid media, the colonies are confined to their starting point. There they deplete the local supply of nutrients which is slowly replenished by diffusive processes. As the colony expands the diffusion to the center becomes less and less to the point that the lack of nutrients causes growth to come to a halt [5]. In this case, only the edge of the colony will have enough nutrients to grow. Thus the growth scales with the circumference of a colony. A linear relation can then be used to describe the expansion, contrary to the exponential relation in liquid media. In this thesis, I only use cells that can passively slide where this linear relation hold. However, it should be noted that many bacterial species have some form of motility that individuals can use to move beyond the

edge of a colony. An overview of the known ways bacteria can move is given by Jarrell and McBride [6].

Pattern formation

Competition experiments are often used to study the dynamics and interactions between species within a biofilm. In such experiments, two or more species are mixed and cultivated together. Competition between species or strains within a biofilm can cause segregation into multiple regions. A colony can start with many small sectors, but this number quickly reduces as the colony expands and one of the species outcompetes its neighbors. Each region can originate from a single parent cell as shown by Hallatschek et al. [5]. Such sectoring of a biofilm can reveal information about many of its features, especially when it comes to the interaction between species and how a colony expands into new territories [7],[8].

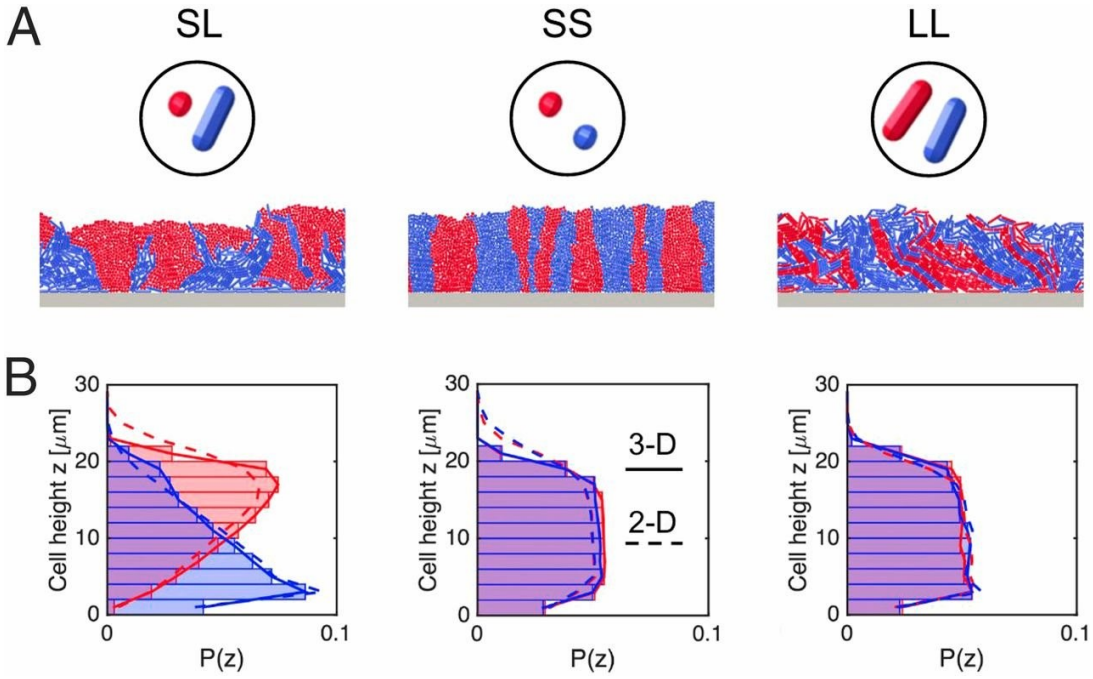

Figure 1.1: The cell shape affects how cells organize in simulations of biofilm growth. **A)** 2D simulations of biofilms. Initial populations were labeled with red and blue and grown at a 1:1 ratio. Different patterns emerge depending on the elongated (long, L) or round (short, S) shapes of the cells. **B)** Distributions of cell positions. P(z) is the volume-weighted histogram of cell z coordinates. The SL mixture forms a layered structure with the long cells laying below the short cells. This layering is absent in homogeneous mixtures (LL and SS). Reprinted figures 2 A and B from [9].

One particular parameter is the cell shape. The effect of cell shape in the vertical direction was studied by Smith et al. [9]. They used an individual-based

computational model describing how the aspect ratio affects the organization of cells. They show that different cell shapes lead to different patterns (Figure 1.1 A). Short cells create straight boundaries and elongated cells create fractal-like patterns. When the two shapes are mixed they separate along the vertical axis (Figure 1.1 B).

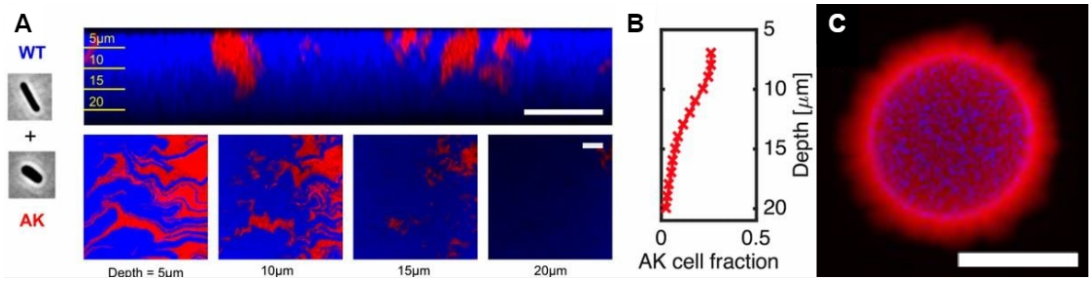

Figure 1.2: Experimental results of short-long competition by Smith et al. match the simulations. **A)** WT (long, shown in blue) strains burrow under AK (short, red) mutants. The top row shows a vertical slice. The bottom row show horizontal slices taken at successive depths. Scale bars are $20\,\mu m$. **B)** The volume fraction of AK cells as a function of depth. The AK cells are more common at the top of the colony. **C)** The colony edge composition is affected by the cell shape. Long (WT, red) cells fully take over from the short (AK, shown in blue) cells on the edge of the colony. The scale bar is $2\,mm$ Figures reprinted from [9]. A is Figure 5 A. B is a cutout of Figure 5 C. C is a cutout of supplementary Figure S12.

Their simulations match the experiment they did afterwards as shown in Figure 1.2 A and B. Here they found both the fractal-like patterns and that the short cells are biased towards the upper layers of the colony. In the supplementary information, they show (Figure 1.2 C) that long cells completely surround the inoculation drop. This implies that the elongated cells have an advantage over the round cells when the colony expands. The main goal of this thesis was to study in more detail how the cell shape gives this advantage to the long cells.

1.2 Thesis outline

In this thesis, I used the same *E. coli* strains as Smith et al.. These strains are the wild-type REL606 (short notation WT) and its mutant REL606 mreB A53K (AK). They are nearly identical apart from their shape [10]. The wild type is much more elongated than the AK type as can be seen in figure 1.3.

Plasmids were added by Smith et al. to make imaging easier. These plasmids cause the expression of either red (RFP) or green fluorescent protein (GFP). They are activated by and offer resistance to the antibiotic kanamycin. I note

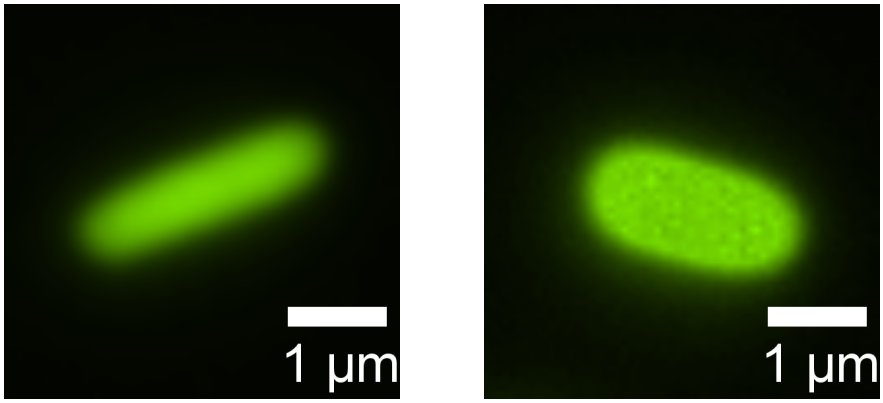

(a) WT-G **(b)** AK-G

Figure 1.3: Micrographs of two strains of E. Coli REL606 mreB. The images were taken by Liselotte Jauffred while the cells were in the log phase of growth. I upscaled the image by a factor of 10 and used an interpolation algorithm to smoothen it. **a)** Wild-type. **b)** AK mutant.

the specific plasmids by a suffix to the strain name with -R for red and -G for green. So the four strains are then WT-R, WT-G, AK-R, and AK-G.

I took the following steps to gain an understanding of the interaction between the two cell shapes.

- At first I discuss how we reproduced that the growth in liquid media was identical for the four different strains as reported by Smith et al. [9] and Monds et al. [10]. On top of that, we quantified the growth in our specific experiment.
- Secondly I discuss how I measured the expansion rates on a surface. I did this for the wild-type and AK mutant independently to see how they compare without interaction.
- After that I explain the main part of the thesis: the competition experiments. Here I show my reproduction and quantification of the pattern formation as shown by Smith et al.. I expanded on this by studying how variations in the initial cell concentration and the ratio between strains affect the pattern formation.
- Finally I share my conclusions and give recommendations for future work.
- There is an appendix at the end of the document with recipes and additional figures. High-resolution versions of figures can be downloaded from `https://sid.erda.dk/sharelink/f2hHPZUpz6`.

Growth rate

2

In this chapter, I study the growth rate of our *E. coli* strains. In the literature, it has been shown that the growth rates in liquid media are practically identical for both strains, although the lag times are shorter for the AK strain [10].

We wanted to reproduce this result and also confirm that the red and green fluorescent labels did not cause a competitive difference. On top of that, we quantified new aspects of the bacterial cells we work with. We measured three different aspects of the growth: the optical density, the cell concentration, and the cell shape and size. The experiments in this chapter were done in collaboration with fellow student Trang Nguyen.

I start this chapter with the necessary theoretical background. This is followed by the experimental methods we used. The last part is dedicated to the measured growth rates and cell shapes.

2.1 Bacterial growth

Bacteria reproduce through a process called binary fission. In this process they first duplicate their DNA, then the cell elongates and finally splits into two identical daughter cells. A controlled, closed, liquid environment is a well-studied example of such growth. In such cell cultures, the population goes through four distinct growth phases as shown in figure 2.1.

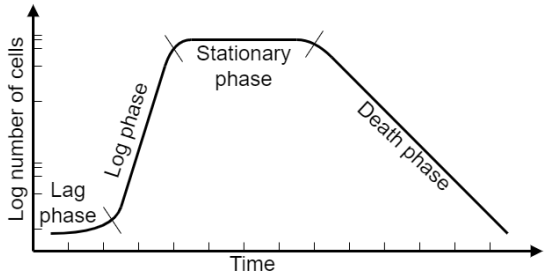

Figure 2.1: Diagram of bacterial growth phases in a closed environment. Reproduced from [11].

The first phase is the lag phase. This is the start-up time during which the bacteria adjust to their new environment and prepare for fast growth. This fast

growth happens in the exponential or log phase where the number of bacteria increases at a fixed growth rate. The name comes from the exponential relation for the population size N:

$$N = N_{t=0} \cdot e^{t \cdot r} \tag{2.1}$$

where $N_{t=0}$ is the quantity at the start of the experiment, t is the time, and r is the growth rate. In the third phase, the environment has changed to the point that the population size becomes stationary. This is caused by either nutrient depletion or toxification from waste produced by the bacteria. The final phase is the death phase where large-scale bacterial death ensues, but without replacement from new cells. The population decrease is also exponential but at a much lower rate than the growth rate.

Measuring population size

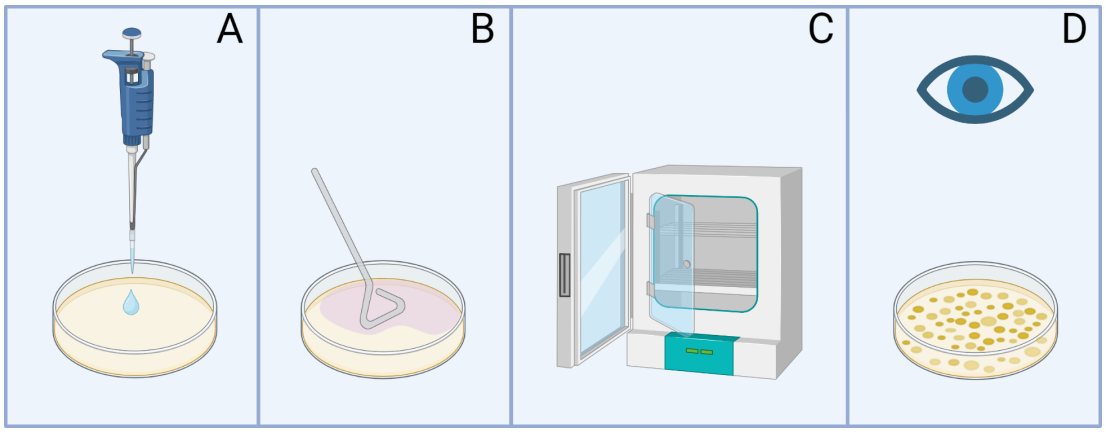

Figure 2.2: A diagrammatic view of the CFU method. **A)** Place a drop of cell culture of a given size and dilution factor on a plate. **B)** Use a cell spreader to homogenously cover the surface. **C)** Incubate until the single cells have grown into visible colonies. **D)** Count the number of colony-forming units.

In this section, I describe two commonly used methods of estimating bacterial population sizes. The first method counts so-called colony-forming units (CFUs). This is visually explained in figure 2.2. It works by spreading a drop of diluted cell culture onto a petri dish with a nutrient-rich substrate. The viable cells on the substrate are left to grow until they form clearly visible colonies. Counting the number of colonies then gives the number of cells in the diluted drop. The concentration of cells in the culture can be calculated from the drop volume, dilution factor, and number of colony-forming units. It is crucial that culture is diluted far enough before spreading to ensure that colonies don't overlap and will be miscounted as only one CFU. The number of cells per petri dish should

be Poisson distributed because the deposition of each cell is an independent event if diluted correctly.

Another way of estimating the population size is by measuring the optical density of a culture. The cell concentration and absorption of light are related through the Beer-Lambert law [12]:

$$\text{OD} = -\log \frac{I}{I_0} = \epsilon \cdot c \cdot l \tag{2.2}$$

Here OD is the optical density, I_0 and I are the incident and transmitted light intensities respectively. ϵ is the attenuation coefficient. It is a media and cell-type specific constant. c is the concentration and l is the pathlength of the light. The linear relation between the cell concentration and optical density makes this method easy to use. It is also much faster to execute than counting colony-forming units. A downside is the necessity of determining the attenuation coefficient for the specific bacterial strain of interest if an exact cell count is desired.

2.2 Methods

Some preparation steps needed to be taken before the interesting experiments could be done In the first step, we made a streak plate for each strain with cells from the frozen stock. We took the cells from the stock in the $-80\,^{\circ}\mathrm{C}$ freezer with the tip of a wooden stick. After that, we streaked them onto minimal media plates in a zigzag pattern as shown in figure 2.3 A. Such plates consisted of minimal media (M63 salt + glucose, recipe in supplementary section 7.2.1) and were solidified with 1.5% agar. It should be noted that all media in this thesis had $30\,\mu\mathrm{m/ml}$ kanamycin in them to prevent contamination and to promote the expression of the plasmids in our strains. Then I placed the plate in an incubator at $37\,^{\circ}\mathrm{C}$ for one night, such that the colonies formed by single cells were visible to the eye. In the end, I placed the plates in a fridge for storage, so they could be used for multiple experiments afterwards.

The next step was to start overnight cultures with the required cell types. We did this by selecting a single colony from a streak plate from the previous step. These cells were then placed in a falcon tube containing $1\,\mathrm{ml}$ of minimal media as shown in figure 2.3. We incubated the culture overnight at $37\,^{\circ}\mathrm{C}$ to ensure there were enough cells to perform an experiment with and to have all of these

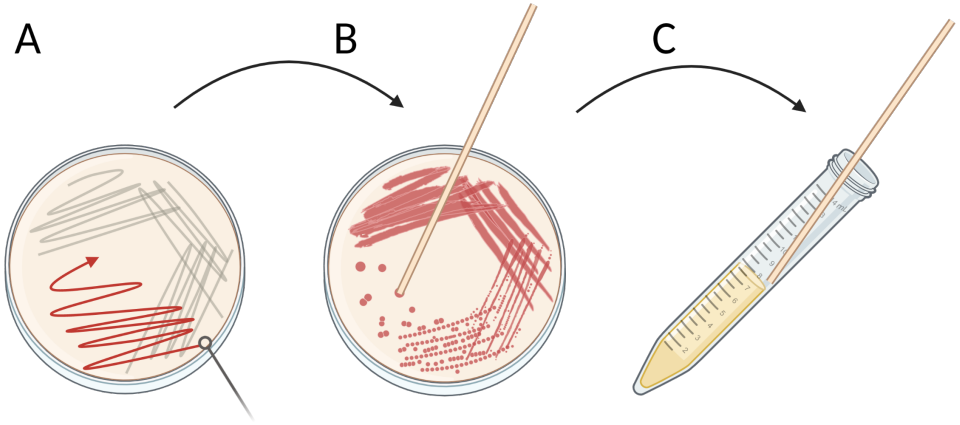

Figure 2.3: Overnight culture preparation. **A)** Streak pattern from frozen stock to grow monoclonal colonies to dilute the cells to the point that a single cell can form a monoclonal colony. **B)** Pick one monoclonal colony after the cells on the steak plate have grown into visible colonies. **C)** Place the cells in a Falcon tube with liquid media. Let the new cell culture grow overnight.

cells in the stationary phase. The tubes were rotated in the incubator to prevent the formation of unwanted biofilms.

In Figure 2.4 I show how we used this overnight culture in our practical implementation of the steps required to measure the parameters of interest. We made a new culture by diluting the overnight cultures by a factor of 100 to a final volume of $5\,\mathrm{ml}$. I.e. we pipetted $50\,\mu\mathrm{l}$ of overnight culture into $4.95\,\mathrm{ml}$ of minimal media. After that, we placed this new culture in the incubator and measured the aforementioned quantities at regular intervals. However, for the shape parameters, we only collected a single time point in the log phase and another in the stationary phase.

Optical density

The optical density was measured with the IMPLEN NanoPhotometer C40 spectrometer. This device measures the OD at $600\,\mathrm{nm}$. For the first time step, we took a sample from the overnight culture. For all time steps after that, we took samples from the new culture.

Colony forming units

In the CFU counting part of our experiment, we aimed for a dilution factor and volume such that the number of cells in the drop was on the order of one hundred. This way the colonies were sufficiently far apart to grow independently, but the count was high enough for an accurate concentration estimation.

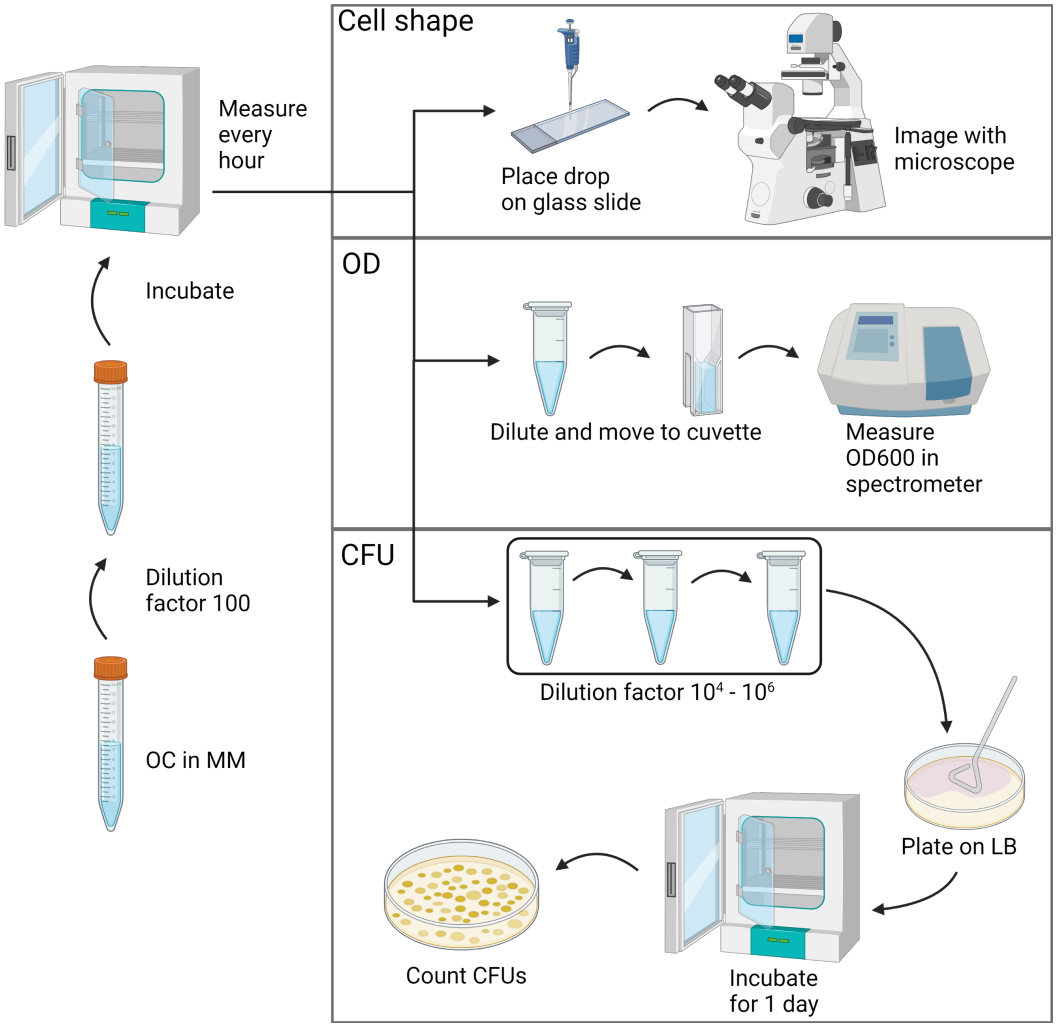

Figure 2.4: A schematic depiction of the experiment. One culture was prepared for all three measurements. Samples were taken from this culture at regular intervals to measure the cell shape, optical density, and number of colony-forming units to determine the concentration.

To achieve this at each measurement time, we took a sample out of each culture and diluted these samples on the order of 10^4 to 10^6 (exact factor depending on cell size and OD). We then spread drops of $100\,\mu l$ onto solid minimal media plates (1.5% agar) and left them in the incubator overnight. This was repeated on three plates for each strain and time to account for random fluctuations in the cell count. Afterwards, we took pictures of the plates and counted the number of colonies. An example plate is shown in Figure 2.5. Finally, we calculated the cell concentration $C = \frac{N \cdot D}{V_{drop}}$, where N is the average CFU count, D is the dilution factor, and V_{drop} is the drop volume.

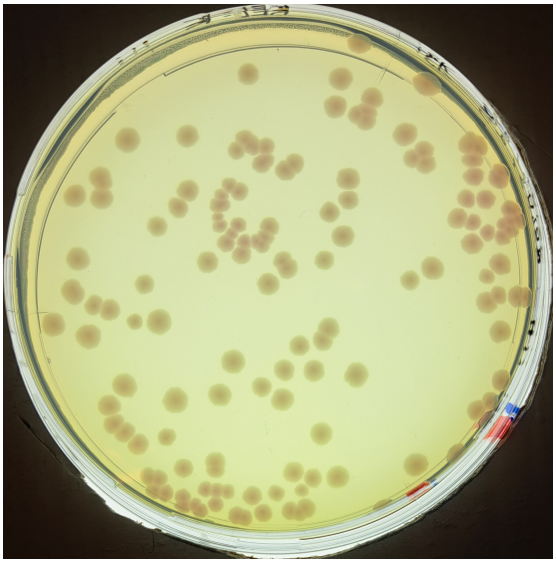

Figure 2.5: An example plate with colony forming units. The medium was minimal media (M63 salt + glucose, 1.5% agar). The strain was wild-type with plasmids expressing red fluorescent protein. The number of colony-forming units was counted as 142.

Cell shapes

For characterizing the cell shapes, Professor Liselotte Jauffred took microscope images of the cells in the log phase and in the stationary phase. She took fluorescence microscope images of the green strains because only the GFP has a bright enough emission to resolve single cells and their shape. For this, she used the Nikon ECLIPSE Ti-timelapse microscope with a 100x magnification oil objective. Images were taken after three hours when the cells were in the log phase and after the second overnight when they were in the stationary phase.

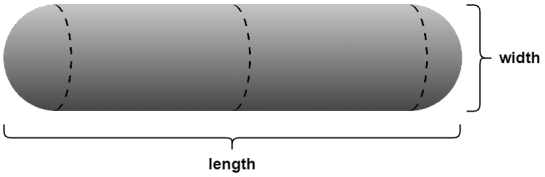

Figure 2.6: A schematic depiction of how I approximate the E. Coli cell shape. It is a cylinder with spherical caps of a given width and length.

I manually measured the length and width (as defined in figure 2.6) of a cell by placing the line tool in Fiji ImageJ along its length or width. The measure button then gives the length of this line. I used these shape parameters to calculate the aspect ratio and volume of each measured cell. The aspect ratio is defined here as the length divided by the width. The volume was calculated by approximating the cells as cylinders with spherical caps as in figure 2.6. This cell volume is

then given by $V_{cell} = \frac{4}{3}\pi(\frac{1}{2}w)^3 + \pi(\frac{1}{2}w)^2(l-w)$, where w is the width and l is the length.

2.3 Concentration results

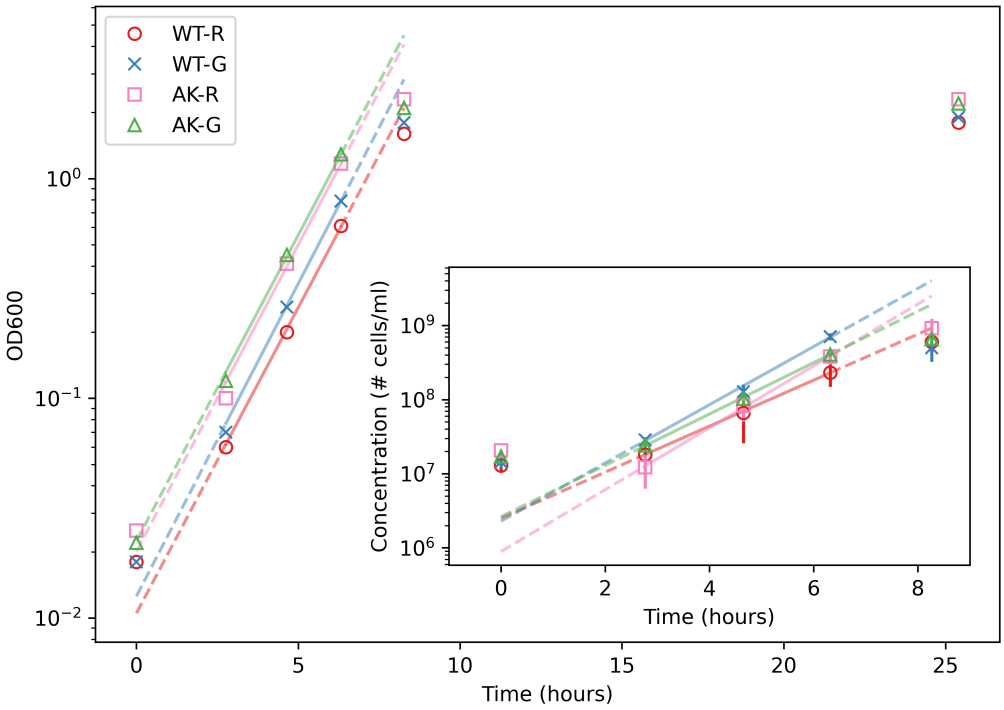

Figure 2.7: The optical density and concentration of the four strains WT-R, WT.G, AK-R, and AK-G as a function of time. **Main figure)** A semi-log plot of the OD of each strain. The solid lines are exponential fits to the data they overlap with. See Table 2.1 for fit parameter results. The dashed parts of the lines are extensions of the fits. **Inset)** The concentration of each strain, as calculated from the average number of CFUs of three plates per time point. The error bars are standard deviations. The fit results are again shown in Table 2.1.

I show the results for the optical density and concentration parts of the experiment in figure 2.7. In both experiments, the four strains (WT-R, WT-G, AK-R, and AK-G) started at similar OD values and concentrations, although the wild-type strains had slightly lower values. In the log phase, there were noticeable differences between the wild type and AK strains. After the log phase, the strains again had similar OD values and concentrations.

We measured the growth rates in the log phase by making exponential fits for both experiments. The used fit function was of the form $A_{t=0} \cdot \exp t \cdot r$, where $A_{t=0}$ is the quantity at the start of the experiment, t is the time, and r is the growth rate. See table 2.1 for the fit results. The solid part of the lines corresponds to

Strain	$OD_{t=0}$	r_{OD} (h^{-1})	$C_{t=0}$ (ml^{-1})	r_{CFU} (h^{-1})
WT-R	1.1×10^{-2}	0.64	2.5×10^{6}	0.71
WT-G	1.3×10^{-2}	0.66	2.3×10^{6}	0.90
AK-R	2.0×10^{-2}	0.64	0.9×10^{6}	0.96
AK-G	2.2×10^{-2}	0.64	2.6×10^{6}	0.80

Table 2.1: Fit results for the exponential phase of the optical density and concentration measurements. $OD_{t=0}$ and $C_{t=0}$ are the optical density and concentration, respectively, at the start of the experiment. r_{OD} and r_{CFU} are the corresponding growth rates.

the data used for the fits. The dashed parts are extensions of the fit results that highlight the longer lag time of the wild-type cells (compared to the AK mutants) but also that both strains grew equally long to reach the stationary phase.

In the OD measurements, the growth rates were practically the same. However, the starting values were quite far apart. The dashed lines show that the short cells entered the log phase almost immediately after pipetting into the new culture, whereas the wild type had a much longer lag time. Of the second overnight culture, only the OD result is shown. The optical density stayed practically constant during this overnight, so we can safely conclude that the culture was in the stationary phase.

The concentration data (inset in figure 2.7) told a more ambiguous story. All strains also showed exponential relations, the fit results are again shown in table 2.1. But there was much more variation and no clear pattern between strains due to large variations in CFU counts.

The relation between OD and concentration is shown in supplementary figure 7.1. It is potentially useful for setting up future experiments but shows no particularly interesting results.

2.4 Cell shape results

Example images of cell shapes in two different growth phases are shown in figure 2.8. It is clear to see that both strains had smaller cell sizes at the later time step. The difference in the number of cells per picture is simply a reflection of the difference in culture concentration. Some of the cells were partially out of focus due to not being aligned with the focal plane. These cells were excluded from the analysis. I quantified the differences in size and shape by measuring

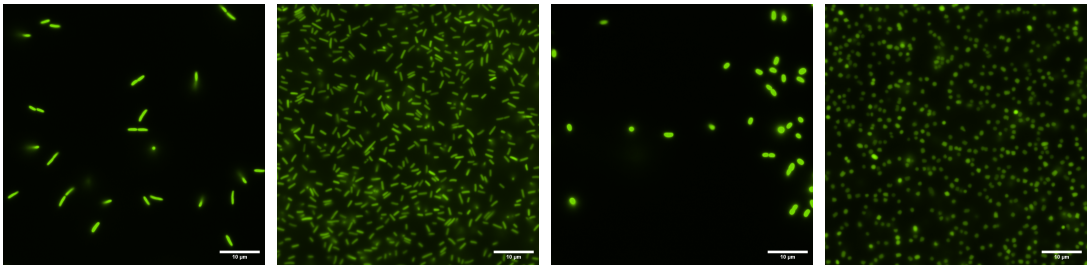

(a) WT-G 3h **(b)** WT-G ON **(c)** AK-G 3h **(d)** AK-G ON

Figure 2.8: Microscope images resolving single cells. The images are of WT and AK cells with GFP markers. Images were taken three hours into the experiment (3h) and after an overnight (ON). Some cells were not parallel to the image plane as is visible from their blurry outline. These should be excluded from the cell shape analysis. The images are cutouts of pictures taken by Professor Liselotte Jauffred. The scale bars are $10\,\mu m$.

the shapes as described earlier in section 2.2. The results are shown in figure 2.9a.

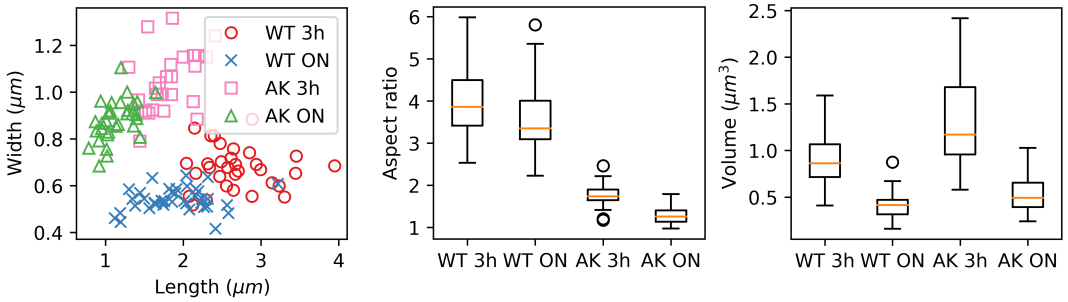

(a) **(b)** **(c)**

Figure 2.9: Cell shape results. N=32 for WT 3h, 39 for WT ON, 25 for AK 3h, and 33 for AK ON. **a)** Cell dimensions. **b)** Aspect ratios (length/width). **c)** Cell volumes.

The strains and time points showed up as four distinct groups. I investigated some features of these groups by calculating the aspect ratio (figure 2.9b) and the volumes (figure 2.9c).

The aspect ratios of the two strains were clearly different. However, they changed only slightly between the log and stationary phases. The volumes displayed much more variation between time points and strains. The first thing to note is that the short cells had a greater volume than the long cells (1.3x for 3h and 1.5x for ON). There was also a big change between the two growth phases. The volumes were reduced by a factor of 2.2 for the long cells and a factor of 2.5 for the short cells.

2.5 Conclusion

We now know the growth rates of the different strains. Interesting to note is the difference in growth rate between the two experiments. They were expected to be similar because the optical density is supposedly linearly related to the cell concentration (see equation 2.2). But instead, we observed that the growth rates from the colony-forming unit experiment were consistently higher than those from the optical density experiment. Regardless of the specific experiment, we found that the different strains grow at similar rates. From this, we conclude that the growth rate in liquid media is independent of strain and plasmid.

The measured aspect ratios are similar to those reported by Smith et al. [9] (4.44 for WT, 2.50 for AK). Small differences in aspect ratios between our and their experiment can be attributed to the different media we used because this can lead to a change of shape as reported by Monds et al. [10]. The nearly constant aspect ratio between the two different growth phases indicates that the bacteria maintain their general shape quite well in a changing environment. The volume on the other hand does change significantly. This change is likely due to reductive divisions that bacterial cells undergo when they enter the stationary phase to reduce the number of chromosome copies per cell [13].

Biofilm expansion rate

3

The growth speed can potentially contribute to a strain's competitiveness in a 2D configuration, but it was thus far unknown how much it differs between the two strains. I measured the growth rate in 2D as the expansion rate of the colonies. This expansion rate was expected to be linear as described in section 1.1.2.

3.1 Methods

The preparation steps for the expansion rate experiment were almost the same as the steps described in section 2.2. The only difference was that I used rich media in the form of lysogeny broth (LB, recipe in supplementary section 7.2.2) for the overnight culture.

I deposited single strain drops with an OD value of 0.6 and a volume of $0.5\,\mu l$ on minimal media plates (M63 + glucose, 1.5% agar). I imaged the colonies at fixed time intervals with a Canon DS6041 digital single-lens reflex camera through a Leica MZ FLIII fluorescence microscope. Afterwards, I analyzed these images with a Python script to extract the surface area.

3.1.1 Pixel size calibration

The pixel size of the images I took was unknown so I had to calibrate them at various magnifications. I did this by taking pictures of a ruler and then measuring the number of pixels per millimeter.

I show how I calibrated the pixels in Figure 3.1. In Fiji ImageJ, I measured the ruler's angle and rotated it such that it would be either horizontal or vertical. Then I saved a slice from this rotated image that only had clear millimeter markers in it. I wrote a Python script to turn this slice into an intensity profile. The shown profile was inverted because originally the black markers showed up as valleys and the areas in between as peaks. The next step was to find the approximate peak positions using SciPy's `find_peaks`. I turned these approximate positions into precise positions by finding the edges of the peaks using SciPy's `peak_widths`. I calculated the peak positions as the middle point between these two edges.

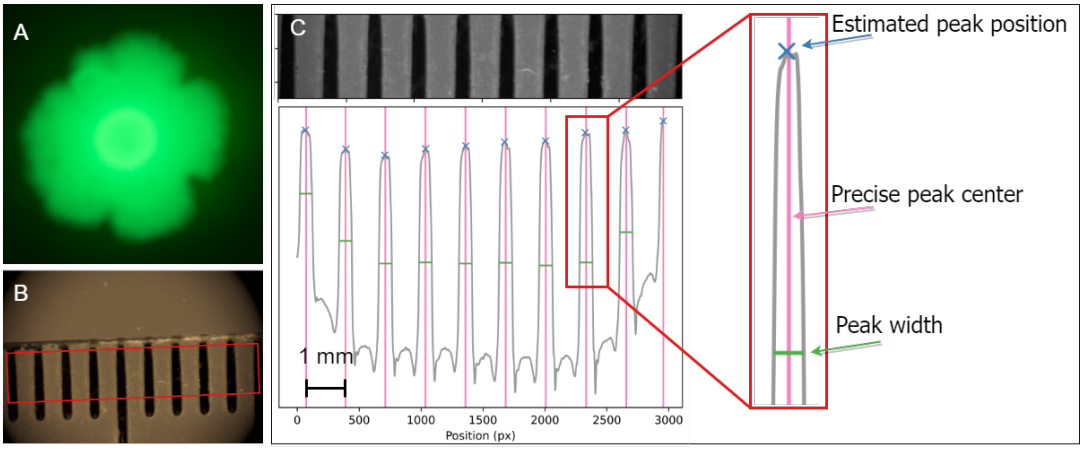

Figure 3.1: Example colony and pixel size calibration method. **A)** Example image of a WT-G colony. **B)** Example ruler image. The red box indicates the cut-out section that is used in the rest of the analysis. **C)** The analysis steps for calibrating the pixel size at a given magnification. The distance between peaks is one millimeter. The approximate peak position, width, and precise position are shown in blue, green, and pink respectively.

With all of the peak positions known, I could determine the number of pixels between peaks. I excluded the peaks at the edge of the images because they appeared to be affected by deformations of the objective. From the remaining pixel distances, I could calculate the mean pixel size.

3.1.2 Surface area

The next step was to find the surface area of each colony at each time point. The images consist of a background and a signal (the colony). I used Otsu's method [14] to separate the two corresponding distributions. This method is useful when it's hard to define the bottom of the valley between two peaks. It can also be extended to distinguish between more than two distributions. In this thesis, I implemented it by using the Python CV2 library [15]. This implementation returns a threshold value that can be used to make binary images. I.e. any pixel with a value greater than the threshold is classified as the analyzed cell type. The threshold for the first time point was constant instead (pixel values of 12 for red and 70 for green). I used the thresholds to turn each image into a binary image.

The contour of the colony followed from using `findContours`. CV2 can easily be used to calculate the area by using `contourArea` and the circumference by using `arcLength`. The steps above work for colonies of any shape, as long as all the parts of the colony are connected to each other. This is especially useful

for the wild-type colonies which typically are not quite circular due to their jagged edges. Finally, I converted the surface areas from pixel counts to mm^2 using the newly calculated calibrations.

3.2 Results

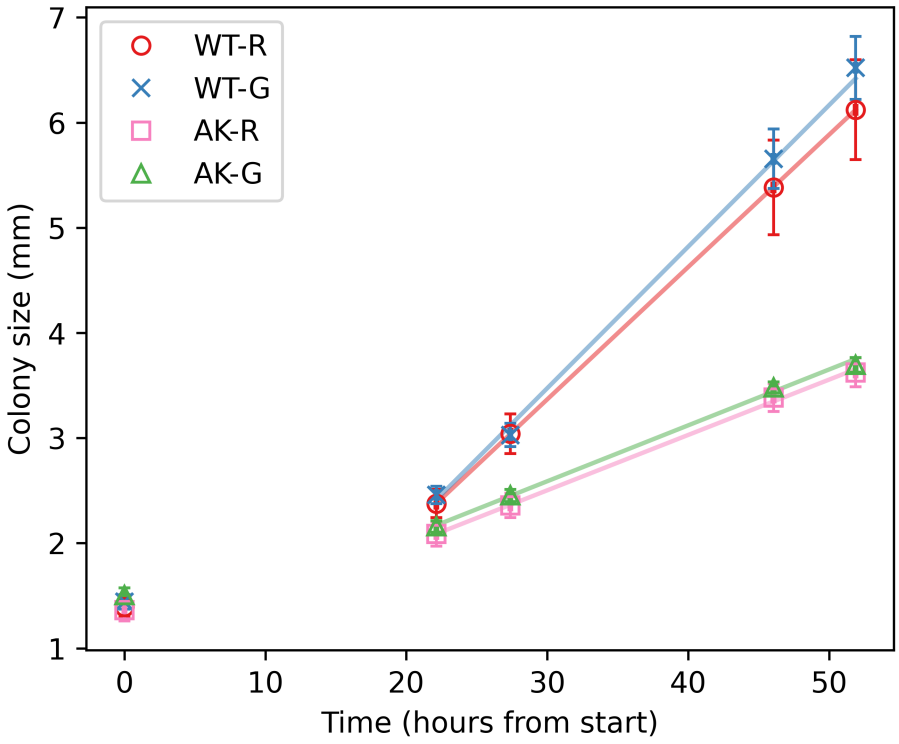

Figure 3.2: Colony size as a function of time. The colony size was defined as the square root of the area. The data points are the average of up to nine colonies for each strain (seven for AK-R). The error bars are standard deviations. The lines are linear fits to the last four data points.

The results for both the horizontal and vertical calibration of each magnification are shown in table 3.1. I used these to calculate the area of each colony at each time.

The mean colony sizes are shown in figure 3.2. This colony size is defined as the square root of the area and functions as an effective radius of the colony. I determined the expansion rate by making a linear fit of the mean colony size. During the first measurement, the cells were still in the lag phase. Therefore I excluded them from the fit.

Magnification	Width (µm)	Height (µm)
0.8x	9.11 ± 0.10	9.10 ± 0.04
1.0x	7.52 ± 0.05	7.50 ± 0.03
1.25x	6.19 ± 0.03	6.20 ± 0.03
1.6x	4.74 ± 0.02	4.75 ± 0.01
2.0x	3.80 ± 0.02	3.81 ± 0.01
2.5x	3.09 ± 0.01	3.07 ± 0.01

Table 3.1: Measured pixel sizes for various magnifications. The values show that the pixels are practically square. The uncertainties are the standard deviations.

I found the expansion rates to be $0.135\,\mathrm{mm/h}$ for WT-G, $0.126\,\mathrm{mm/h}$ for WT-R, $0.053\,\mathrm{mm/h}$ for AK-G, and $0.053\,\mathrm{mm/h}$ for AK-R.

3.3 Discussion and conclusion

The growth rates were the same for all strains in liquid media (chapter 2). But on a surface it is clear that the long wild-type cells grow more than twice as fast as the AK strains. This outcome highlights the difference between the two environments. Apparently, the cell shape creates a competitive edge in the environment that physically limits growth. We can take a look at how the strains compete now that we know how they perform relative, but independent of each other. This is the main topic of this thesis and I will show my work on this in the next chapter.

Competition experiments 4

In this chapter, I discuss everything related to my competition experiments. I start with an explanation of the tools I used. This is followed by an explanation of the basic methods. I then describe the basic experiment and its specific settings. I expand on that by varying some of the experiment parameters. The chapter ends with a quick look into the dynamics of the competition between the two strains.

4.1 Imaging tools

To see how the two strains interacted when they competed, I needed a way to image colonies at a high resolution and a way to distinguish between the two strains within such colonies.

4.1.1 Fluorescent labels

One way of distinguishing between different parts of a sample is by using fluorescent labels. Fluorescence happens when a molecule is excited due to the absorption of a photon of energy $h\nu$ and emits a photon at a lower energy $h\nu'$, where h is the Planck constant and $\nu > \nu'$ are the frequencies of the photons. The absorption and emission wavelengths are specific to a given molecule.

This can be used in microscopy by labeling specific parts of a sample with such fluorescent markers. The sample can be illuminated with the excitation wavelength of the marker. The fluorescence light is then sent through a filter matching the emission wavelength. This way only the labeled parts are imaged and all other light (noise) sources are filtered out.

This method has been seen widespread use in recent years due to the development of tools based on the green fluorescent protein (GFP). This protein was first discovered in jellyfish and has a well-understood mechanism for fluorescence. The genetic code of organisms can be modified to express the protein, thus making it a useful tool in practically all living things. A great number of variants have been engineered for increased brightness and stability. Fluorescent

proteins have also been designed for many different excitation and emission wavelengths. This makes it possible to use multiple colors in one experiment to mark different regions. [16]

Two commonly encountered challenges of fluorescent labels are bleaching and phototoxicity. Bleaching happens when the fluorescent proteins are altered by the photons that hit them. This can decrease or remove their fluorescence. In practice, this usually happens when a sample is exposed for a long time or by a bright source. Phototoxicity is the term used for a (negative) change in the physiology of the sample. The high-intensity illumination required to excite the fluorescent proteins can be absorbed by other cell components. This can lead to degradation of some organic molecules. In other cases, such molecules can react with oxygen. That in turn produces reactive oxygen species (ROS). ROS are known to negatively affect many processes in living matter. A more thorough overview is given by Icha et al. [17]. They also provide a reference card with steps to reduce the impact of phototoxicity in experiments.

4.1.2 Confocal laser scanning microscopy

For the high-resolution imaging, I used a confocal laser scanning microscope. A confocal microscope is a special type of light microscope. Its illumination and detection are limited to one point on the sample instead of a large area by use of a focused beam or laser. The light coming from the sample passes through a pinhole. Correct placement of the pinhole eliminates out-of-focus light. This combination of pinhole and focused beam allow for a high resolution at the point of interest while also reducing the noise from out-of-focus light resulting in higher contrast. This is particularly useful in fluorescence microscopy where a sample should be illuminated as little as possible (see section 4.1.1).

A sample needs to be scanned in a raster pattern to create a complete image because only one pixel is illuminated at a time. One key advantage compared to traditional microscopy is that this raster is not limited to the horizontal axes, but can also be used for collecting a so-called Z-stack. Here the sample is scanned along the vertical axis. This makes it possible to construct 3D images [18].

A laser is used as the light source because it is a coherent light source that is easy to focus. It is also convenient in combination with fluorescence microscopy due to its narrow wavelength band.

4.2 Methods

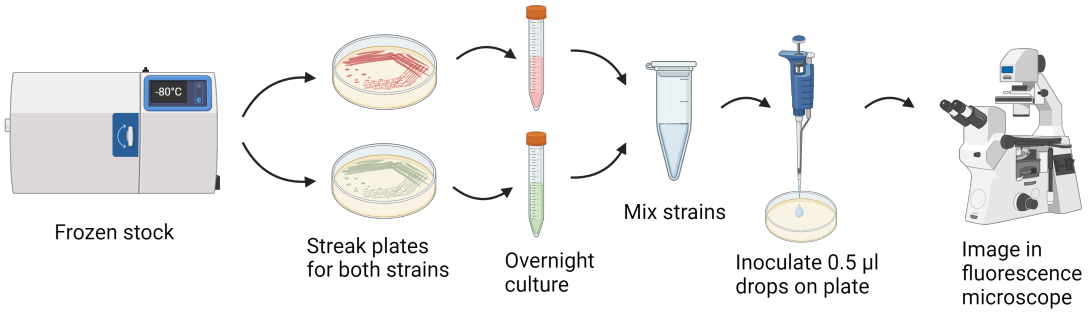

Figure 4.1: A diagram of the steps for a surface competition experiment. From left to right: A droplet of bacteria is taken with a wooden stick from the frozen stock to make streak plates on minimal media (MM M63 + glucose, $30\,\mu g/ml$ kanamycin, 1.5% agar). From a streak plate, one monoclonal colony is transferred into 2 ml of LB supplemented with kanamycin. This culture is grown overnight with the cap open to allow for oxygenation. Afterwards, the cell concentration is estimated by measuring the OD600 value of the culture (not shown). The steps above are taken for each strain (WT-G, WT-R, AK-G, and AK-R). Each strain is diluted and mixed to the desired ratio and concentration. A drop of $0.5\,\mu l$ is placed on a minimal media plate. This plate is incubated for x hours. Finally, the colony is imaged in a fluorescence microscope.

In Figure 4.1, I show how I performed the competition experiments. The first steps were similar to the preparation steps in chapters 2 and 3. I grew the overnight cultures in rich media (lysogenic broth, see supplementary section 7.2.2) instead of minimal media.

In the last preparation step, I inoculated a drop containing the mixture of desired cells on a minimal media plate and let this new colony grow overnight. I adjusted the concentration of the strains in the drop for the specific experiment by first measuring the optical densities (OD600) of the overnight cultures using the IMPLEN NanoPhotometer C40. Following that, I diluted the strains into an Eppendorf tube and mixed them thoroughly using a Labnet VX-200 vortex mixer.

The dilution depends on the desired total volume V_{final}, optical density OD_{final}, and ratio between the two strains $part_A$:$part_B$. From this, the volumes V_A, V_B, and V_{LB} of strain A, strain B, and the media can be calculated using equation 4.1.

$$V_A = \frac{OD_{final}}{OD_A} \cdot \frac{part_A}{part_A + part_B} \cdot V_{final} \tag{4.1a}$$

$$V_B = \frac{part_B}{part_A} \cdot \frac{OD_A}{OD_B} \cdot V_A \tag{4.1b}$$

$$V_{LB} = V_{final} - V_A - V_B \tag{4.1c}$$

Finally, I deposited drops from the mixture of either 0.5 µl or 1 µl on a minimal media (M63 salt + glucose, 1.5% agar) plate. I incubated this plate for up to 36 hours such that the colonies had grown to a point that they could be imaged with a fluorescence microscope afterwards.

Imaging

I imaged the colonies with a Leica DMI6000 CS SP5 confocal laser scanning microscope. In this microscope, I used a wavelength of 488 nm to excite the green fluorescent protein (Lonza pmaxGFP) and a wavelength of 543 nm for the red fluorescent protein (Evrogen pTurboRFP). The RFP had an optimal excitation wavelength of 509 nm and an emission wavelength of 574 nm. The laser wavelength (543 nm) did not quite match that of the excitation. This created a need for a higher signal amplification than for the GFP (typical gain of 600 to 700 V) For GFP it was 487 nm and 553 nm respectively (typical gain of 350 to 450 V).

I used a 5x magnification objective as this objective offered a high level of detail while providing a large enough field of view to fit (almost) an entire colony in one image. Images were scanned at a size of 512x512 pixels with a scan speed of 400 Hz. The pixel size was 6.0665 µm so the images' sides had a length of 3.1 mm I extended the scan to the vertical direction by making a z-stack. I set it up to take 11 steps of 10 µm to ensure that the colony surface was fully imaged, but not bleached by overly long imaging times. I repeated these z-stacks for the red and the green channels separately.

4.2.1 Image preprocessing

The confocal microscope images needed to be processed before I could systematically quantify features. I chose to identify each pixel as being either red or green to simplify the quantification. In this section, I describe how I prepared the images before I could apply this classification.

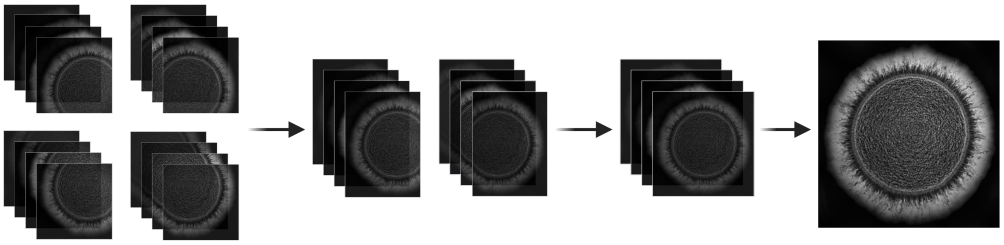

Figure 4.2: Stitching process of multiple images into a full colony image. I used the pairwise stitching plugin in Fiji ImageJ [19] to first stitch the two upper corners together with the lower corners. Then I stitched the resultant left and right halves of the image to create the full colony image. In the case of z-stacks, I made a maximum-intensity projection as explained in Figure 4.3.

Stitching (optional)

In some cases, colonies had grown to a size where they could not fit in a single confocal microscope image. In those cases, I took four images and stitched them together using the pairwise stitching plugin in Fiji ImageJ [19]. I took multiple steps as shown in the left side of figure 4.2 because this algorithm can only stitch two images/image stacks at a time.

Maximum intensity projection (optional)

A high-resolution image can be created from a z-stack by selecting the pixels on the surface of the colony. These pixels are the brightest pixels in the stack due to how a confocal microscope works. The z-positions outside of the colony will not reflect light and therefore be dark. The light to and from positions deeper in the colony will be partially blocked by cells on the surface, depending on how opaque they are. Regardless, they will be imaged as less intense than the surface pixels. This makes it possible to create a maximum-intensity projection from a z-stack.

I implemented these projections in a Python script that loops through all the pixels of an image and for each pixel picks the brightest value from the z-stack and saves this value to create a new image. This image consists of the best-focused pixels and yields the sharpest result. I show this schematically in figure 4.3.

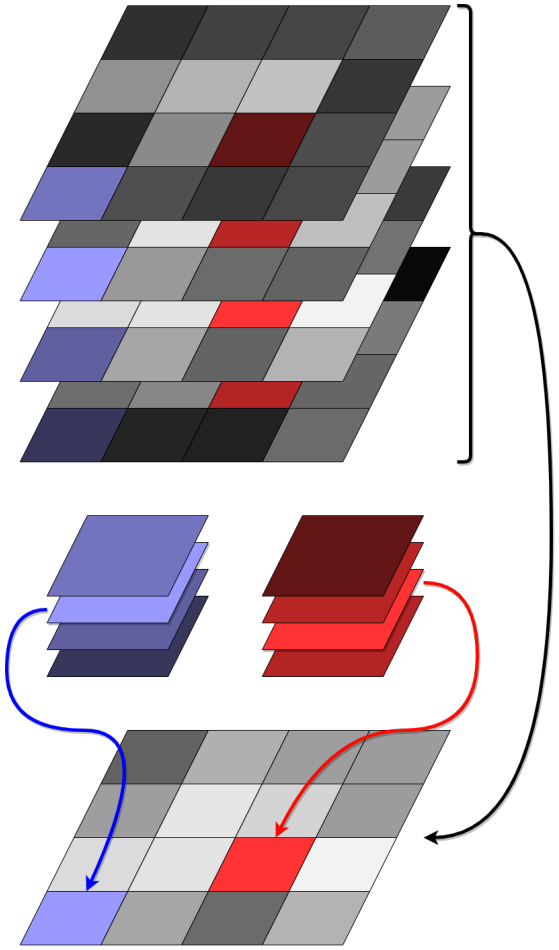

Figure 4.3: The maximum intensity projection process. Each pixel was treated as an individual stack. The brightest layer in this stack was saved as the pixel value in the final image. The pixels in the final image can come from multiple layers. For example for the blue pixel, the second layer from the top is the brightest, whereas it is the third layer for the red pixel.

Colony contour & homeland circle

Each colony had several easily detectable regions. Here I define my terminology for each of these parts, see Figure 4.4 for reference. The 'homeland' is the randomly mixed center of a colony from where the biofilm expands (inside the yellow circle). This area roughly corresponds to the inoculation drop. It is surrounded by thin rings that I call the 'coffee stain' because of its resemblance. The region beyond this is the 'growth region'. Here the cells appeared to be expanding into new territory without much distortion due to the initial deposition on the surface. This is also the region where the patterns of interest were most visible.

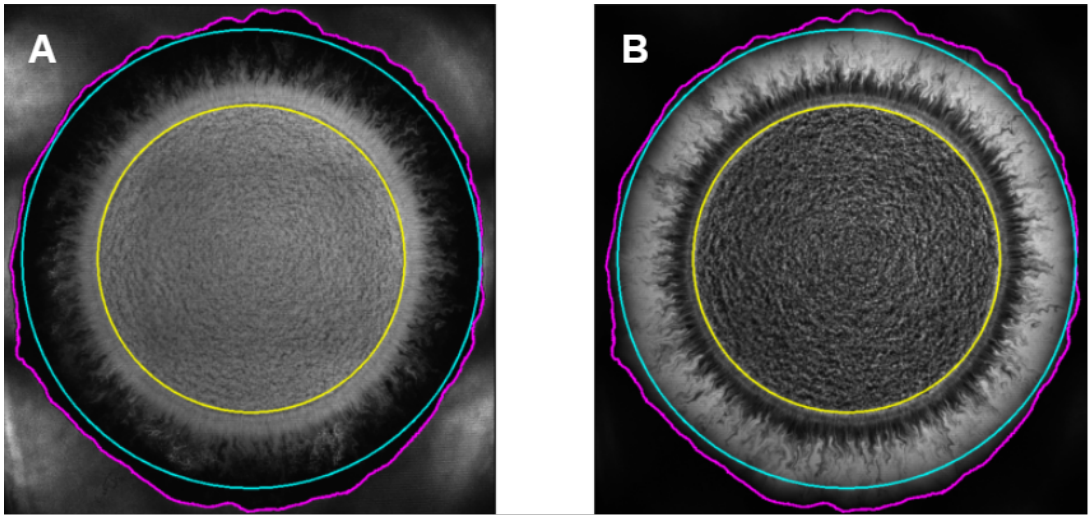

Figure 4.4: Example images of a WT-G + AK-R colony with the homeland circle (yellow), colony contour (magenta), and maximum analyzable radius (cyan) drawn on top. **a)** Red channel, used for detecting the colony contour. **b)** Green channel, used for finding the homeland circle.

The next step was to find the start and end points for different parts of the radial analysis. I.e. find the center and nearest edge of a colony. I found the homeland circle by manually adjusting the radius and center coordinates until the circle visually matched the homeland edge in the green channel. The minimum distance between the colony center and the colony edge was found by first detecting the contour of the colony. I did this by thresholding the red channel image and then applying the CV2 function find_contours() to this binary image. Finally, I evaluated the distance between each point on the contour and the homeland center. The shortest distance was saved as the maximum distance for the radial analysis.

I saved all tunable and extracted parameters in a metadata file specific to the analyzed image. Some applications of the contour apart from finding the maximum radial distance could be the removal of the image background or a calculation of the colony's surface area.

4.2.2 Pixel classification

The last preprocessing step is the assignment of pixels to one of the possible cell types (e.g. WT-R or AK-G). The first step for this classification is to calculate the pixel intensity distribution of an image. This distribution consists of two peaks. A background distribution made up of light emitted and reflected by the cells of the color that is not imaged, agar, and generic background noise. And a signal

peak emitted by the cells of the color that is imaged. I again used Otsu's method [14] to classify the pixels (see section 3.1.2).

In practice, this classification is not easy due to the large intensity variations of the various parts of the colony. The thin layer at the edge is dim whereas the homeland edge is very bright. The different colonies and strain combinations also all express different intensities and were imaged with slightly different settings. These variations make it impossible to use a fixed threshold for all images because too many image features would be lost.

Making intensities comparable

I tried various ways to make all pixels comparable for use in a thresholding algorithm. Here I present the two most successful options. In the first method, I select circles centered on the homeland center. Each circle is rescaled to use the full range of possible pixel values. I do this by finding the highest pixel value in a circle and then multiplying all values in the circle by the same value such that the new maximum is 255 (8-bit). E.g. if the original maximum value is 198 then all values will be multiplied by a factor of $\frac{255}{198}$. This method can be extended to the minimum values as well, but that was unnecessary for my images. One advantage of this method is that both color channels can be analyzed separately and then compared.

In Figure 4.5 I show two examples. In the first example (Fig. 4.5a) the fractal-like patterns quickly faded out with the radius of the colony. The background in the four corners was quite bright but was not processed at all, so it could be safely ignored. The circularly rescaled version (Fig. 4.5b) shows the fractal-like patterns at all distances. This image yields a high-quality binary image (Fig. 4.5e). However, there are also some problems with this method. One of them is that this method can not deal with intensity variations that exist along a different axis than the radius. For example, most images have an intensity gradient from the top right to the bottom left. Another issue is that this method breaks down in extreme situations such as shown in Figure 4.5c where some of the circles are rescaled too much because even the brightest pixel is quite dim. This creates unwanted artifacts, especially visible as circles in the binary image (Fig. 4.5e).

In the other method, I made pixels in different parts of an image comparable by dividing one color channel by the other. We expect each pixel to be occupied by either one or the other imaged species. I.e. a dark pixel in one channel should correspond to a bright pixel in the other. If a bright pixel is divided by a dark pixel

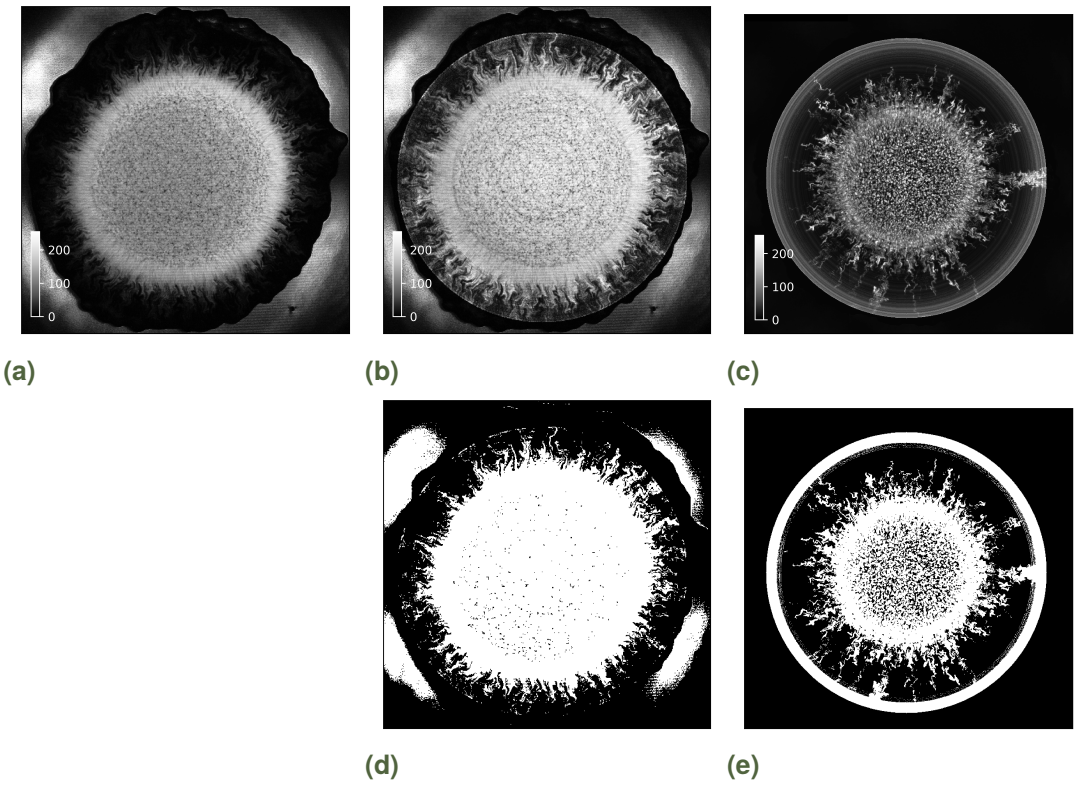

Figure 4.5: Examples of the circle rescaling method. The colony images are from experiments described in section 4.3. **a)** Original red channel image of a WT-G + AK-R colony. **b)** Circularly rescaled version of a) as described in the main text. **c)** Binary image of b). **d)** Circularly rescaled version of the green channel of a WT-R + AK-G colony. **e)** Binary image of d).

it will result in a large value, and a small value will be found if the brightness is inverted. This amplifies the difference between the pixel values of the two channels. This method works well in areas with significant intensity variations.

Before dividing, I added a constant to all pixel values in both channels. So for a given pixel, the division would be $\frac{A+c}{B+c}$, where A and B are the pixels from channel A and B respectively, and c is the shift constant. The Taylor expansion for large c is $1 + \frac{a-b}{c} + \mathcal{O}((\frac{1}{c})^2)$. This shows that it is essentially a subtraction of channel B from channel A. That is another way of amplifying the differences between the two channels. It works especially well close to the homeland where the intensities are relatively homogenous. In my method, I used an intermediate value that is of the same magnitude as the pixel intensities.

I show an example result of such a divided and subtracted image in Figure 4.6c. For the thresholding, I limited the analysis to a donut-shaped disk with its inner radius corresponding to the homeland radius and its outer radius being the maximum analyzable radius minus 25 pixels. The minus 25 is to exclude

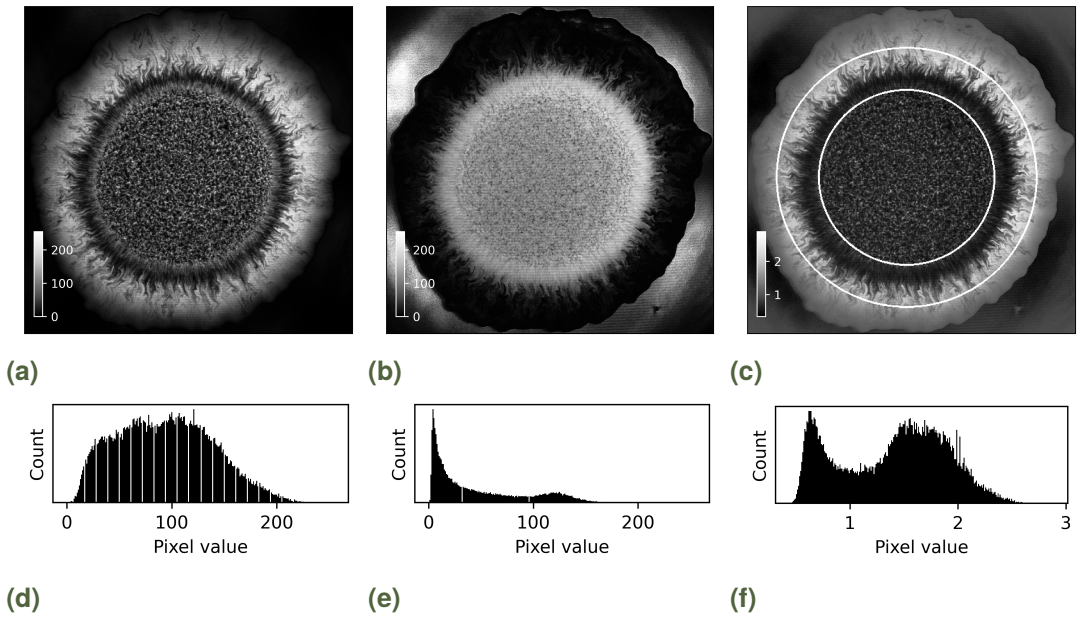

Figure 4.6: Examples of using the division method prepare for thresholding. The same WT-G + AK-R colony as in Figure 4.5 a, b, and d was used. **a)** Green channel. **b)** Red channel. **c)** Green channel divided by red channel. I added 100 to both channels before dividing. I used the area between the circles to create the histogram in f). **d-f)** Histograms of the pixel intensities within the donut regions indicated in a-c). Note that d) and e) have a pixel value range from 0 to 255, whereas f) has a much shorter range due to the division.

artifacts at the far boundary. The new radius serves as the real maximum analyzable distance.

The histograms in Fig. 4.6d and 4.6e consist of a signal peak and a background from many different sources. In contrast, the two peaks in Fig. 4.6f correspond to the two color channels and can easily be separated. From these histograms, it is evident that it would be much easier for Otsu's method to separate the distributions of the two colors from each other, compared to separating the signal in one channel from the background.

Another advantage of this method is that the background noise existing in both channels is mostly divided out. This means that gradients or stitching artifacts do not affect the binary image. The effectiveness of this method is visible from the binary image in Figure 4.7. It captures a high level of detail in the patterns. However, it does lack some of the levels of detail that the binary images of the circle rescaling provide. Between the two methods, I prefer the division over the circular rescaling because the reduction of artifacts makes it more consistent over all the imaged colonies.

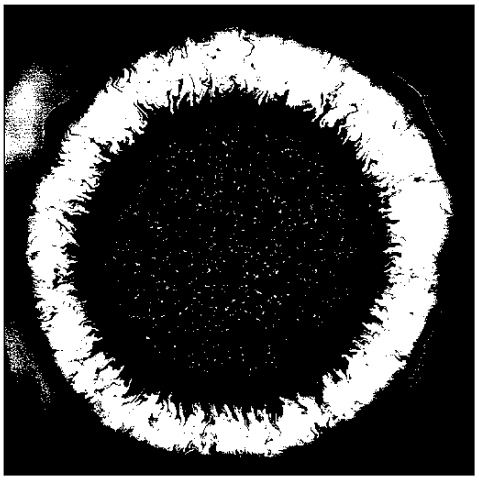

Figure 4.7: Binary image of Figure 4.6c. The main patterns are visible and do not suffer from imaging artifacts.

4.3 Results

4.3.1 Competition between bacteria of different aspect ratios

My initial experiments were based on the protocol described in Silja Svendsen's BSc thesis [20] to be sure that initial parameters were chosen such that interesting features would be visible in the imaged colonies. The default OD of the mixed drop was 0.6 and the strains were mixed at a 1:1 ratio. I imaged the colonies as described before in section 4.2.

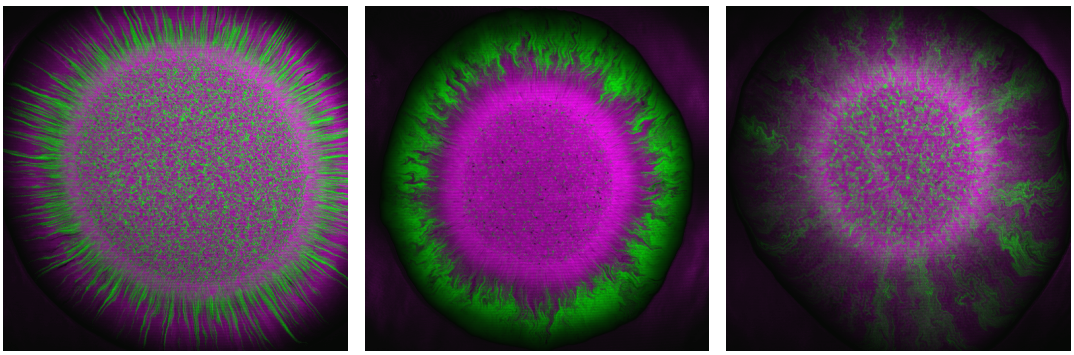

(a) AK-G + AK-R **(b)** WT-G + AK-R **(c)** WT-G + WT-R

Figure 4.8: Images of colonies with different cell-type combinations after growing for over twenty-two hours. They are false-color composites of the two channels. Magenta corresponds to RFP and green to GFP.

I show example results of all three interesting strain combinations in figure 4.8. Qualitative differences are immediately clear by eye: the AK-AK combination produced straight spiked patterns, whereas the other combinations produced more fractal-like patterns. When the elongated cells competed against each other they performed roughly equally well and formed fractal-like patterns. This is different for the long-short combination where AK was dominant in the area of the initial drop, but the long cells took over as the colony grew outwards. The opposite color combination (not shown) showed similar patterning but with the colors inverted. Similar patterns were observed by Smith et al. [9] where they explained it by using the cell shape in a computational model.

4.3.2 Feature quantification

I extracted multiple quantitative measures from the binary images by processing circles of increasing sizes. These measures could then be analyzed as a function of distance from a colony's center or homeland edge. I show an example of a binary circle in figure 4.9 to illustrate how I define the quantities.

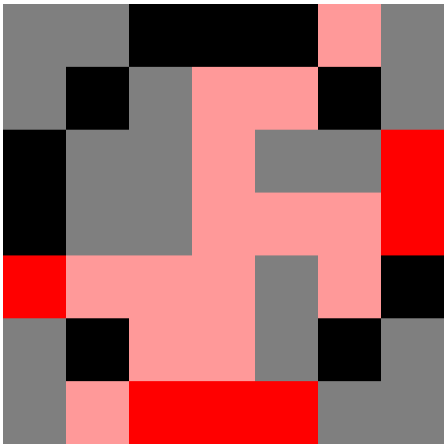

Figure 4.9: Example of a binary circle from a colony. The red and pink pixels represent cells. Black and gray represent the background. On this circle 6 of the 16 pixels are classified as cells, therefore the occupied fraction is 0.375. There are three sectors, of length 1, 2, and 3 (no unit).

Fraction occupied

The first measure is the fraction of pixels occupied by the given cell type (see Fig. 4.9 for an explicit example). This feature gives an indication of which cell type is dominant at what distances. To calculate the average over multiple colonies I had to shift the fraction series such that their homeland edges aligned. This way

I account for variations in drop size, thus making the series of different colonies comparable.

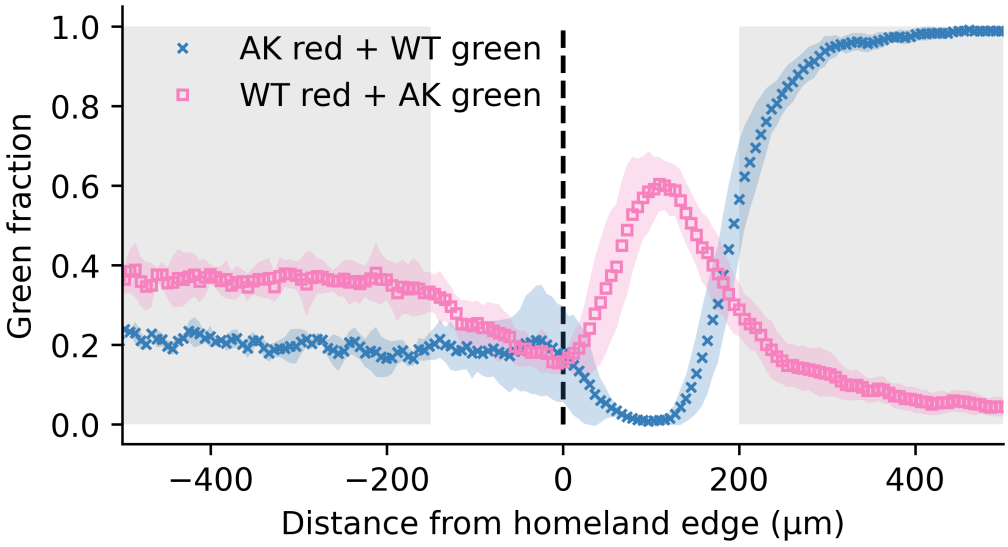

Figure 4.10: The mean fraction of green pixels as a function of distance from the homeland edge for different cell combinations (N=3 for AK-R+WT-G, N=5 for WT-R+AK-G). The shaded areas correspond to one standard deviation. The gray and white areas correspond to the three different regions I discuss in the main text. A reduced range is displayed in the plot because both ends of the series suffered greatly from noise (due to low pixel count for small circles in the homeland, and due to many incorrectly classified pixels close to the colony edge).

I show the average result of multiple strain combinations in figure 4.10. Each series goes through three distinct regions as the radial distance increases (from left to right):

- The inoculation drop where both strains are mixed. Here the fraction is almost constant with some small fluctuations due to the randomness of the mixing.
- A region close to the homeland edge where the occupied fractions fluctuate greatly. We refer to this region as the coffee stain. In section 4.4 I give more context for this terminology.
- An outer region where the long wild-type cells take over from the shorter AK mutants as the distance from the colony center increases.

I observed this behavior for both AK-R + WT-G and the opposite color combination WT-R + AK-G. The series I show in Figure 4.10 are not exact mirror images of each other. One cause of this could be the different levels of fluorescence expression in each strain. Differences could also be caused by how

the two channels are measured. Especially close to the homeland edge, it was difficult to classify all pixels correctly due to the abundance of both strains. But despite these differences, it is clear that the elongated wild-type cells completely outperform the short AK cells in the long run.

Sectors

I also quantify the patterning by looking at the sectors. I define a sector as a group of consecutive identical pixels following the circumference of the circle. Again, explicit examples are given in Figure 4.9.

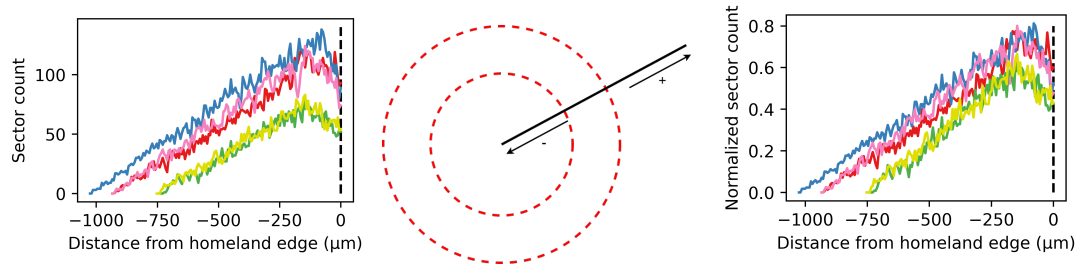

Figure 4.11: An explanation for my choice of sector count normalization. **a)** Sector counts of five colonies of the WT-R+AK-G combination with an OD of 0.6 and a 1:1 ratio. Each color represents a different colony. The black dashed line represents the homeland edge. In this example, the biggest colony had a radius of over one millimeter (blue) whereas the smallest was about 25% smaller (green). **b)** The red dashed circles represent the homeland edges of two different colonies. Each dash represents a sector. The black line is the radial axis. **c)** Normalized sector count version of a).

On top of shifting all series to the homeland edge, I had to apply a normalization step to make the different colonies comparable. The number of sectors on a circle in a randomly mixed region scales linearly with the circumference of this circle as I show in figure 4.11a. I assume that the sector density at the homeland edge is nearly independent of the circle radius due to an abundance of cells. This means that if a colony is twice as big as another, it will also have approximately twice the number of sectors at the same distance from the homeland. For example see Figure 4.11b where I show two hypothetical homeland edges with the same sector densities. The solution I used for this was to divide the sector counts by the homeland radius. This way each colony would have comparable sector counts. I show how this brings the counts of different colonies closer together in Figure 4.11c.

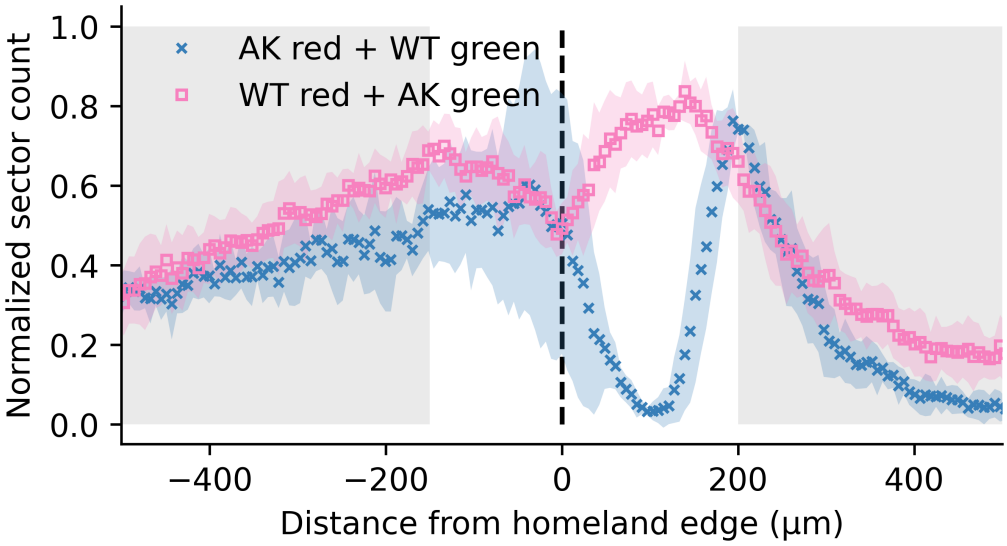

Figure 4.12: The mean number of sectors as a function of distance from the homeland edge for different cell combinations (N=3 for AK-R+WT-G, N=5 for WT-R+AK-G). The shaded areas are standard deviations. The counts were normalized as described in the main text. The gray and white areas correspond to the three different regions I discuss in the main text. A reduced range is displayed in the plot because both ends of the series suffered greatly from noise (due to low pixel count for small circles in the homeland, and due to many incorrectly classified pixels close to the colony edge).

I show the average result for multiple strain combinations in figure 4.12. Again, each series goes through three distinct regions as the radial distance increases (from left to right):

- The inoculation drop where the sector count increases linearly with the radius in the randomly mixed homeland.
- A region close to the homeland edge where the sector counts fluctuate greatly.
- An outer region where the number of sectors drops to zero as sectors are ended until only one big sector remains where one of the cell types dominates.

The sector count does not look at a specific color. Instead, it only counts how often the two strains alternate along the circle. This is evident from how similar the data of the two opposite color combinations are. They are only different close to the homeland region where, as explained before, the classification of pixels is difficult.

4.3.3 OD variations

I investigated the effect of the number of cells in the inoculation drop by varying the concentration. I combined the long (green) and short (red) cells at a one-to-one optical density ratio. This solution had an OD value of 0.1. I diluted parts of this first solution by a factor of 10 and a factor of 100 to make new solutions with an effective OD of 0.01 and 0.001 respectively. I inoculated, grew, and imaged multiple colonies per solution as described in section 4.2.

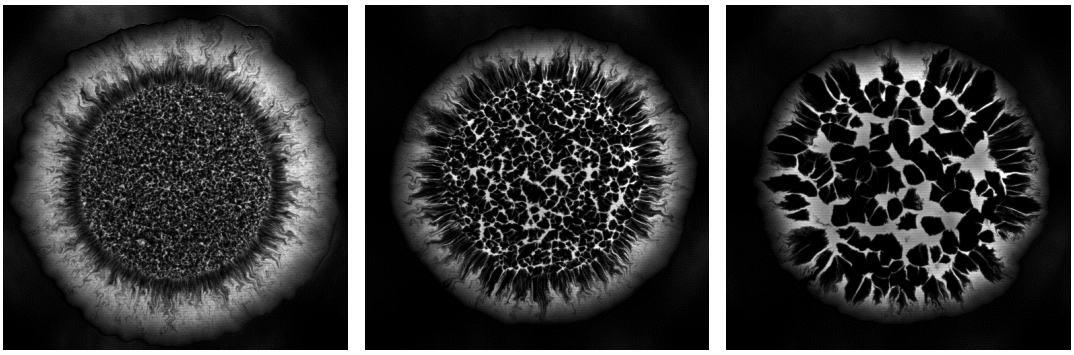

(a) OD = 0.1 **(b)** OD = 0.01 **(c)** OD = 0.001

Figure 4.13: Example images of the green channels of WT-G+AK-R colonies with various initial optical density values.

In figure 4.13, I show an example colony for each of the OD values. From the images, it is clear that the number of sectors in the homeland reduces with reducing OD. I.e. the sector count scales proportional to the number of cells deposited. Note that the dark sectors form islands made up of short AK cells. These islands are surrounded by seas of long cells that even form thin channels. Another thing to note is that the coffee stain becomes harder to spot and the patterns in the growth region change drastically. The abundant fractal-like patterns at high concentrations become scarce and are mostly replaced by straight sector borders. Although they do still exist in places where the sectors are thin and alternate quickly between the two strains. My first impression is that the long cells take over at the far end of the growth region, independent of the inoculation concentration.

I quantified this the same way as in section 4.3.2 and show the results in figure 4.14. The first thing to note is that the low-concentration colonies did not expand nearly as far as the higher concentrations, despite growing for the same duration. For this reason, I will not consider the results of OD 0.001 in the rest of the discussion.

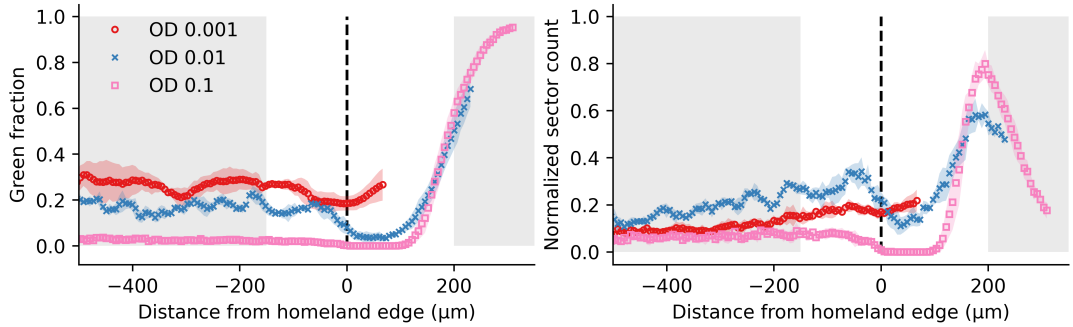

Figure 4.14: Quantitative results for various OD values of WT-G+AK-R colonies. Both figures show the means of multiple colonies (N=6 for OD 0.1, 3 for OD 0.01, and 5 for OD 0.001). The shaded areas correspond to one standard deviation. The gray and white areas correspond to the three different regions. The dashed black line indicates the homeland border. **Left)** The fraction of green pixels as a function of distance from the homeland edge. **Right)** The normalized number of sectors as a function of distance from the homeland.

The occupied fraction convincingly shows that the long cells overtake the short cells, similar to what happens in Figure 4.10. This is independent of the concentration. The same can be seen for the sector counts where the dips and peaks match up. However, the counts fluctuate less for the lower concentration.

4.3.4 Ratio variations

Another parameter I varied is the solutions' long-to-short cell ratio. This was to see at what limit the elongated cells would no longer win the competition. The experiment again followed the same steps as in section 4.2, but with a target OD value of 0.3. The ratios I tested were 1:1, 1:9, 1:99, and 1:999. Keep in mind that these ratios are based on the measured optical densities and do not reflect cell counts. Trang Nguyen (unpublished) measured that the cell concentration in the stationary phase was more than twice as high for the wild-type cells when measured at the same OD as the AK mutants. Regardless, the ratio decrease between experiments is independent of this because I used the same cell cultures for each of them.

In Figure 4.15, I show an example colony for each ratio. The homeland becomes darker as the number of elongated, green cells decreases with increasing ratio. In the growth region, the long cells become visible for all ratios, although it takes longer for the more extreme ratios. The fractal-like patterns are visible in all colonies. Images 4.15c and especially 4.15d display an additional pattern in the

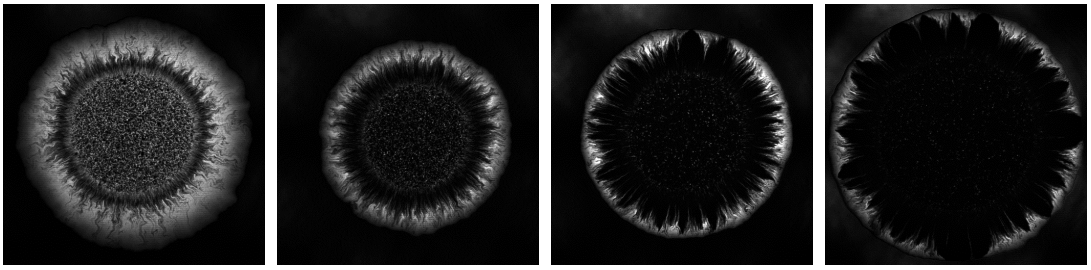

(a) 1:1 **(b)** 1:9 **(c)** 1:99 **(d)** 1:999

Figure 4.15: Example images of the green channels of WT-G+AK-R colonies with various initial ratios (long:short).

form of dark cone-shaped regions where the long cell sectors curve around the round cells.

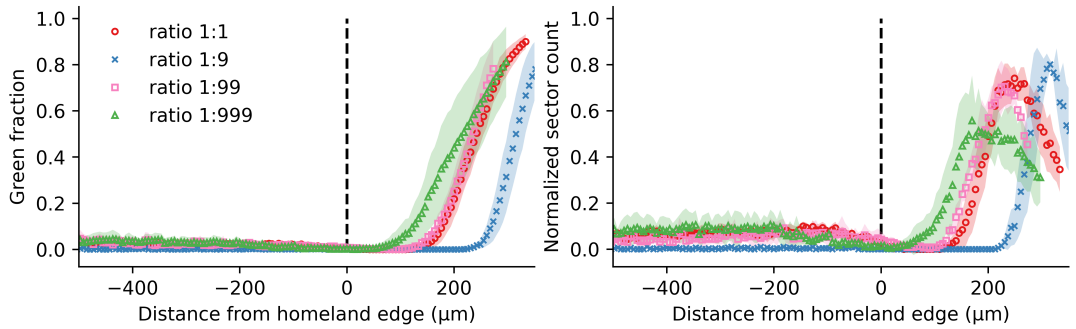

Figure 4.16: Quantitative results for various ratios of long:short of WT-G+AK-R colonies. Both figures show the means of multiple colonies (N=5 for 1:1, 3 for 1:9, 3 for 1:99, and 4 for 1:999). The shaded areas correspond to one standard deviation. The dashed black line indicates the homeland border. **Left)** The fraction of green pixels as a function of distance from the homeland edge. **Right)** The normalized number of sectors as a function of distance from the homeland.

In Figure 4.16, I again show the occupied fraction and sector count as a function of distance. The fraction series all start close to zero, but peak shortly after entering the growth region. The sector count series also support the story that the elongated cells take over as they peak at a similar distance where the fraction starts to rise, and then drop as sectors are being closed off (AK) or connected (WT). The only difference between the various ratios was the distance from the homeland edge at which they started certain trends (e.g. takeover by the green pixels in the fraction occupied plot or the peak positions of the sector counts). Altogether it is quite surprising to see that the elongated cells so consistently manage to reach the colony's edge where they can outperform the short cells.

4.4 Zooming in on the pattern formation

In this section, I present a brief study of a colony's growth dynamics at a smaller scale than those studied so far. Both by using greater magnification objectives in the microscope and by reducing the timescale to the order of hours or minutes instead of days. This was to gain an understanding of how the patterns form and to take a closer look at potential underlying mechanisms that cause this formation. Furthermore, it is a potential starting point for future research.

In the first part, I looked at how the patterns formed on a large scale. In the second part, I looked at a level of detail where individual cell interactions were visible.

4.4.1 Pattern formation

The reason to look into a colony's dynamics is not only to see how a colony formed but also to confirm that the pattern freezes shortly behind the growth front as described in section 1.1.2. The coffee stain is one of the specific patterns of which I wanted to see the formation because until this experiment we had no way of knowing how this circle formed so consistently. The last area of attention is the colony edge where the patterns are actually formed as it expands into new territory.

Methods

The process leading to the colony inoculation was the same as in previous competition experiments. I used an inoculation drop with an OD of 0.6 and a ratio of 1:1. After inoculation, I placed the plate in the $37\,^{\circ}\mathrm{C}$ incubator for 2.75 hours to ensure that the cells would be past the lag phase. I imaged the colony at one-hour intervals with the Nikon ECLIPSE Ti-timelapse microscope. This microscope uses filters to select a fitting bandwidth from a white light source to excite and detect the emission from the fluorescent molecules. A Nikon FITC filter was used for GFP (excitation 467 to $498\,\mathrm{nm}$, emission 513 to $556\,\mathrm{nm}$) and a Nikon Texas Red filter for RFP (excitation 542 to $582\,\mathrm{nm}$, emission 604 to $644\,\mathrm{nm}$). At each time point, I took a z-stack with a step size of $7\,\mu\mathrm{m}$. The temperature of the plate was maintained at $37\,^{\circ}\mathrm{C}$ during and in between imaging. Afterwards, I used a function in the Nikon microscope software to select the best-focused planes.

Results

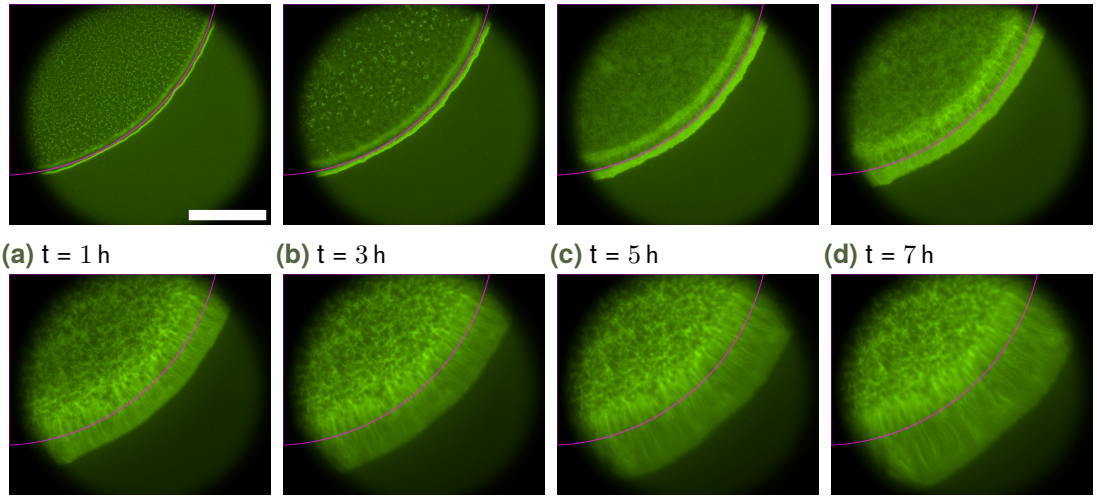

(a) t = 1 h **(b)** t = 3 h **(c)** t = 5 h **(d)** t = 7 h

(e) t = 9 h **(f)** t = 11 h **(g)** t = 13 h **(h)** t = 15 h

Figure 4.17: Colony pattern formation visualized by timelapse microscopy. A WT-G+AK-R colony was imaged once per hour. Only the green channels of the odd hours from the start are shown. The scale bar is $250\,\mu m$ wide. The purple line indicates the homeland edge at the start of the experiment. See the supplementary folder 'Timelapse 20x' for all time frames, channels, and full resolution.

In Figure 4.17, I show some of the frames from the timelapse. From the first frames, we can see that the colony started with a mostly empty homeland (i.e. low intensity and corresponding cell density) surrounded by two thin rings that form the initial coffee stain. As time progresses, these rings broaden, become less sharp, and expand both inwards and outwards. The inwards expansion eventually stops as the homeland fills up (i.e. high density). The outwards expansion continues throughout the whole experiment and creates familiar fractal-like patterns. The pattern freezes quite close behind the colony edge (about 50-100 µm from the front). The colony expanded by about $230\,\mu m$ in sixteen hours. So it had an expansion rate of about $14\,\mu m/h$.

Discussion and conclusion

This is much slower than what I measured for the expansion rates in chapter 3 ($0.13\,mm/h$ for WT and $0.05\,mm/h$ for AK). The slower growth is likely due to the sub-optimal environment in the microscope incubator. One indication of this worse environment was that the agar had shrunk visibly between the start and end of the timelapse. This was likely due to the agar drying out. Another cause could be excessive phototoxicity due to long imaging times in the z-stack.

Despite this slower growth, I still gained insight into the formation of the coffee stain. We now know that there is a coffee stain from the very start of the experiment and that the final circular pattern stems from this initial circle. The formation of this coffee stain is likely due to how the particles are moved to the edge of the inoculation drop when it dries [21]. However, the final pattern is quite different from that at the start due to growth. On top of that, I have confirmed that the pattern freezes shortly after the colony has expanded into new territories.

4.4.2 Intracellular interaction

In this section, I look at intracellular interactions by looking at how the single cells move relative to each other. If the pattern formation is purely due to physical interactions as described by Smith et al. [9], then that should be visible. I also did this experiment with the purpose of opening up new approaches to studying the pattern formation.

Methods

For this proof of concept experiment, I took the same steps as for the previous experiments, but I used an undiluted overnight culture of WT-G (OD = 4.42) + AK-R (OD = 4.64). These were mixed at a 1:1 ratio. I then inoculated a $0.5\,\mu m$ drop onto a minimal media plate.

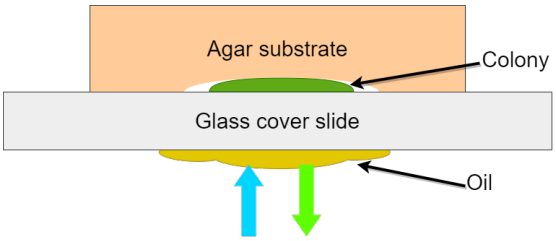

Figure 4.18: Diagram of the sample used to image individual cells in the timelapse microscope. The colony grew between the agar substrate and the glass cover slide. The arrows underneath represent the excitation and emission light of the fluorescent markers.

The new part of this experiment was to cut a slab of agar out of the plate and deposit it onto a glass cover slide with the colony facing the glass. See Figure 4.18 for a schematic view of the sample. This allowed me to use a 100x magnification oil objective in the timelapse microscope. I took a timelapse z-stack with nine steps of $0.3\,\mu m$ at ten-minute intervals immediately after inoculation.

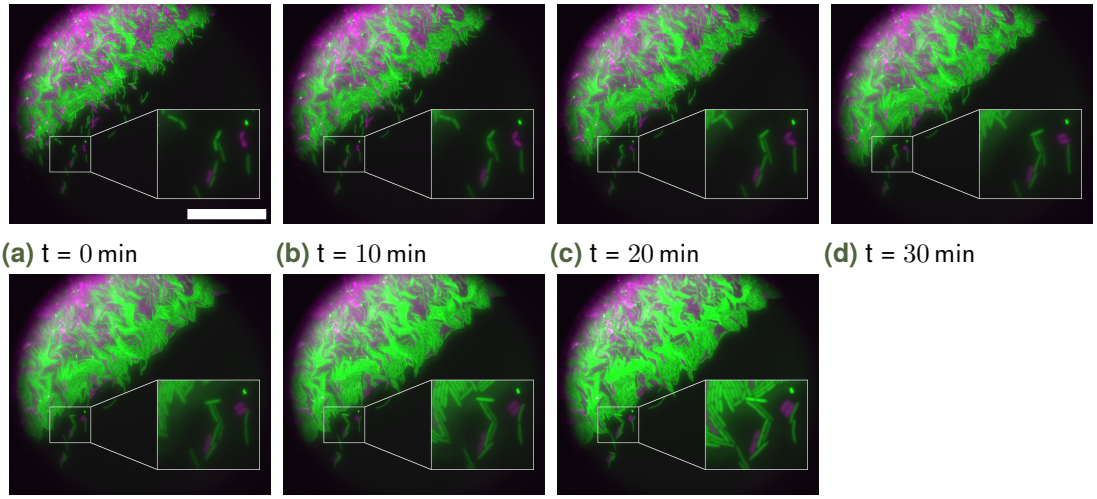

(a) t = 0 min **(b)** t = 10 min **(c)** t = 20 min **(d)** t = 30 min

(e) t = 40 min **(f)** t = 50 min **(g)** t = 60 min

Figure 4.19: Individual cell interactions visualized by timelapse microscopy. A WT-G+AK-R colony was imaged at ten-minute intervals. The images are false-color composites of both channels. The red AK cells are shown in magenta. The scale bar is 50 µm wide. The highlighted area was enlarged 2.5x. See the supplementary folder 'Timelapse 100x' for full-resolution images.

Results

I show the frames of this timelapse in Figure 4.19. The green wild-type cells were more common than the short cells close to the colony edge. They became even more dominant as time progresses. Some cells were in front of the colony from the start, which was likely due to how the agar was slightly dragged over the glass slide during deposition. This would result in some cells being left behind. A few parts of the images became unclear as the colony grew. I assume that this was due to cells being pushed up into a second layer and thus moving out of focus.

Cells aligned with each other all over the place. It seems to me that the long cells aligned more and faster than the short cells. In some cases, the alignment had no clearly visible cause, even lonely cells that divided into two aligned next to each other (e.g. see enlarged area).

Altogether I have shown that this imaging method works and presents many features to study. It can already be used to learn some things about the alignment of the different cells. But mostly it is a good starting point for future research.

Conclusion

5

The goal of my research was to gain a better understanding of how bacterial cell shapes affect pattern formation in biofilms and to quantify the competition between shapes. I started by measuring the growth and expansion rates for the long and short strains and found that the long-cell colonies expand more than twice as fast on a surface ($0.13\,\mathrm{mm/h}$ for WT vs $0.05\,\mathrm{mm/h}$ for AK) despite having the same growth rate in liquid media as short cells (r_{OD} of $0.65\,\mathrm{h}^{-1}$ for WT vs $0.64\,\mathrm{h}^{-1}$ for AK). After that, I performed the basic competition experiments and found that different cell shape combinations generated different patterns. Smith et al. noted in their supplementary information that the presence of the long cells became more dominant close to the colony edge as the difference in size increased relative to the short cells. This is also what I found in my experiments. Additionally, my experiments showed that whether the long cells won the competition or not was independent of the cell concentration at inoculation. However, the formed patterns in the colony did change with lowering concentration as larger and larger sectors appeared, especially in the homeland. The most surprising result came from my variation of the initial ratio of the two strains. Here I found that even at a 1:999 (long:short) ratio, the long cells overcome their disadvantage and take over as the colony expands.

Some of the experimental and analysis procedures could be improved and lead to new insights with more time spent on them. For example, the colonies could have grown for a longer time so the whole time evolution would be visible. On top of that the radial intensity fading would likely be a smaller factor in the analysis because all analyzed parts of the colony would be in a stationary phase after depleting the local supply of nutrients. Another thing that could be investigated is the effect of vertical layering on the imaging. Smith et al. [9] reported that the round cells grow on top of a colony, thus hindering the imaging of the long cells underneath. This means that the actual sectoring in a colony could be different from what I imaged. Layering could also play a role in the competition because the long cells grow closer to the substrate. This gives them better access to nutrients and might allow them to grow faster. My last suggested area of improvement regards the pixel classification as it proved difficult to accurately display all patterns in the binary images. The challenge is still in how the pixel

intensities can be made comparable between color channels and different areas of a colony.

From the similar growth rates but different expansion rates, I conclude that the long cells have an advantage when growing on a surface. This also matches how the elongated wild-type cells completely outperform the short AK mutants in the competition experiments. However, the perseverance of the wild-type at an extreme disadvantage implies that the difference in expansion rate might not be the explanation for this phenomenon. Instead, both the expansion rate and patterning could be caused by an underlying mechanism. In section 4.4 I presented a way to study the interactions of individual cells with timelapse microscopy. I believe that this could be a good starting point to look further into how cell shape affects competition and growth. Another direction could be a study of how competition affects growth in three dimensions. Comparing the two environments could result in insights into if/how attachment to a surface plays a role in pattern formation. For more long-term research, it might be interesting to investigate how the cell shape and corresponding patterns affect genetic diversity within a biofilm and how that affects antibiotic resistance.

Bibliography

6

[1] Byung Hong Kim and Geoffrey Michael Gadd. *Bacterial Physiology and Metabolism*. New York: Cambridge University Press, 2008.

[2] Olivier Tenaillon, David Skurnik, Bertrand Picard, and Erick Denamur. „The population genetics of commensal Escherichia coli“. In: *Nature Reviews Microbiology* 8.3 (2010), pp. 207–217. DOI: 10.1038/nrmicro2298.

[3] Patrick Daegelen, F. William Studier, Richard E Lenski, Susan Cure, and Jihyun F. Kim. „Tracing ancestors and relatives of *Escherichia coli* B, and the derivation of B strains REL606 and BL21(DE3)“. In: *Journal of Molecular Biology* 394.4 (2009), pp. 634–643. DOI: 10.1016/j.jmb.2009.09.022.

[4] Hans-Curt Flemming, Jost Wingender, Ulrich Szewzyk, Peter Steinberg, Scott A. Rice, and Staffan Kjelleberg. „Biofilms: an emergent form of bacterial life“. In: *Nature Reviews Microbiology* 14.9 (2016), pp. 563–575. DOI: 10.1038/nrmicro.2016.94.

[5] Oskar Hallatschek, Pascal Hersen, Sharad Ramanathan, and David R. Nelson. „Genetic drift at expanding frontiers promotes gene segregation“. In: *Proceedings of the National Academy of Sciences* 104.50 (2007), pp. 19926–19930. DOI: 10.1073/pnas.0710150104.

[6] Ken Jarrell and Mark McBride. „The surprisingly diverse ways that prokaryotes move“. In: *Nature reviews Microbiology* 6.6 (2008), pp. 466–476. DOI: 10.1038/nrmicro1900.

[7] Lukas Eigentler, Fordyce A. Davidson, and Nicola R. Stanley-Wall. „Mechanisms driving spatial distribution of residents in colony biofilms: an interdisciplinary perspective“. In: *Open biology* 12 (12 Dec. 2022), p. 220194. DOI: 10.1098/rsob.220194.

[8] Carey D. Nadell, Knut Drescher, and Kevin R. Foster. „Spatial structure, cooperation and competition in biofilms“. In: *Nature Reviews Microbiology* 14.9 (2016), pp. 589–600. DOI: 10.1038/nrmicro.2016.84.

[9] William P. J. Smith, Yohan Davit, James M. Osborne, Wook Kim, Kevin R. Foster, and Joe M. Pitt-Francis. „Cell morphology drives spatial patterning in microbial communities“. In: *Proceedings of the National Academy of Sciences* 114.3 (2017), E280–E286. DOI: 10.1073/pnas.1613007114.

[10] Russell D Monds, Timothy K Lee, Alexandre Colavin, Tristan Ursell, Selwyn Quan, Tim F Cooper, and Kerwyn Casey Huang. „Systematic perturbation of cytoskeletal function reveals a linear scaling relationship between cell geometry and fitness“. In: *Cell reports* 9.4 (2014), pp. 1528–1537. DOI: 10.1016/j.celrep.2014.10.040.

[11] Sushil Humagain. *Growth of Bacteria and the Bacterial Growth Curve*. https://onlinesciencenotes.com/growth-of-bacteria-and-the-bacterial-growth-curve/. Accessed: May 9, 2023. Aug. 2018.

[12] J.A. Myers, B.S. Curtis, and W.R. Curtis. „Improving accuracy of cell and chromophore concentration measurements using optical density“. In: *BMC biophysics* 6.1 (2013), p. 4. DOI: 10.1186/2046-1682-6-4.

[13] Thomas Nyström. „Stationary-Phase Physiology“. In: *Annual Review of Microbiology* 58.1 (2004). PMID: 15487934, pp. 161–181. DOI: 10.1146/annurev.micro.58.030603.123818.

[14] Nobuyuki Otsu. „A Threshold Selection Method from Gray-Level Histograms“. In: *IEEE Transactions on Systems, Man, and Cybernetics* 9.1 (1979), pp. 62–66. DOI: 10.1109/TSMC.1979.4310076.

[15] G. Bradski. „The OpenCV Library“. In: *Dr. Dobb's Journal of Software Tools* (2000).

[16] Måns Ehrenberg. *The green fluorescent protein: discovery, expression and development*. Scientific Background on the Nobel Prize in Chemistry 2008. Oct. 2008.

[17] Jaroslav Icha, Michael Weber, Jennifer C. Waters, and Caren Norden. „Phototoxicity in live fluorescence microscopy, and how to avoid it“. In: *Bioessays* 39.8 (Aug. 2017). DOI: 10.1002/bies.201700003.

[18] James Pawley. „Handbook of Biological Confocal Microscopy“. In: 3rd. Springer, 2006, pp. 4–5.

[19] Stephan Preibisch, Stephan Saalfeld, and Pavel Tomancak. „Globally optimal stitching of tiled 3D microscopic image acquisitions“. en. In: *Bioinformatics* 25.11 (Apr. 2009), pp. 1463–1465. DOI: 10.1093/bioinformatics/btp184.

[20] Silja X. P. Svendsen. „How single cell shape affect spatial patterning in microbial communities - A lattice model“. MA thesis. Niels Bohr Institute, University of Copenhagen, 2022.

[21] Peter J. Yunker, Matthew A. Lohr, Tim Still, Alexei Borodin, D. J. Durian, and A. G. Yodh. „Effects of particle shape on growth dynamics at edges of evaporating drops of colloidal suspensions“. In: *Physical Review Letters* 110 (3 Jan. 2013). DOI: 10.1103/PhysRevLett.110.035501.

[22] Nathanael van den Berg. *Thesis preparation project report*. Niels Bohr Institute, University of Copenhagen. 2022.

Supplementary information 7

7.1 Figures

High-resolution and extended versions of figures and images can be found at `https://sid.erda.dk/sharelink/f2hHPZUpz6`.

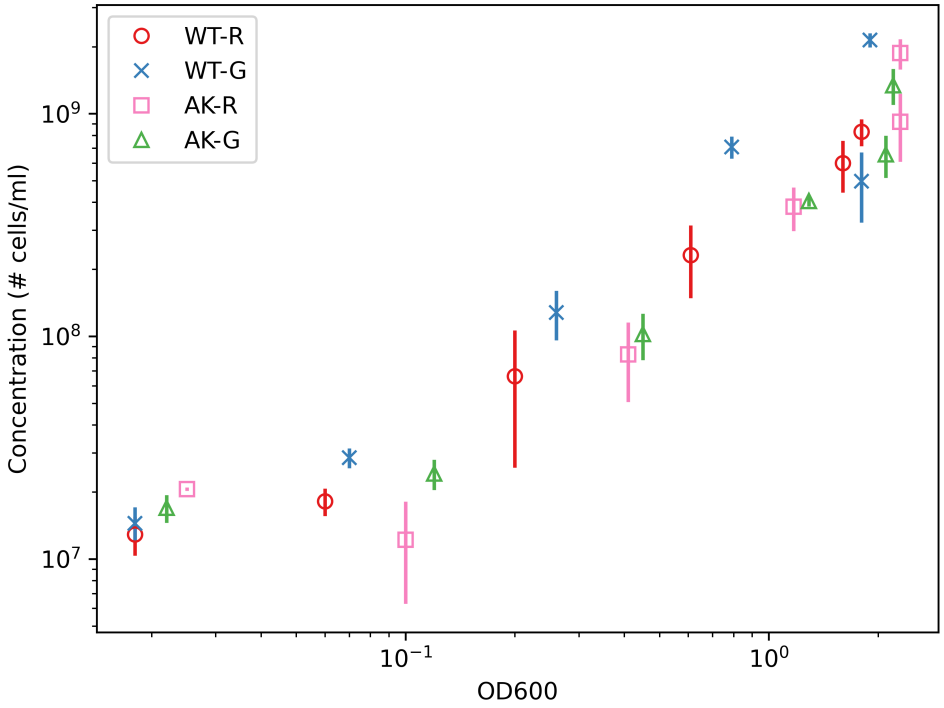

Figure 7.1: Cell concentration as a function of optical density for all four strains used in this thesis. It can be useful as a reference for experiments.

7.2 Media recipes

Note: these recipes are mostly the same as in my thesis preparation project [22]. For the solid version used to make plates: add $3.75\,\mathrm{g}$ of agar (before autoclaving).

7.2.1 Minimal media (250 ml) (M63 + glucose)

Minimal media are media designed to provide organisms with the minimal required necessities for growth. The specific minimal medium used in this thesis is optimized for *E. coli*. Below I describe how to prepare the medium.

- Take 200 ml milli-Q water
- Autoclave the mixture
- Add 50 ml of 5x M63 salt
- Add 250 µl of 1 mg/ml B1
- Add 500 µl of 1 M $MgSO_4$
- Add 2.5 ml of 20% weight/volume glucose stock solution
- Add 250 µl kanamycin (30 mg/ml)
- Mix everything with a magnet stirrer

7.2.2 LB (250 ml)

LB stands for lysogeny broth (but is also known as Luria–Bertani medium). It is a nutritionally rich medium designed for bacteria. Below I describe how to prepare the medium.

- Take 250 ml milli-Q water
- Add 2.5 g Bacto Tryptone
- Add 1.25 g Bacto yeast extract
- Add 1.25 g NaCL